Balanced dual acting compounds targeting aromatase and estrogen receptor α as an emerging therapeutic opportunity to counteract estrogen responsive breast cancer

Balanced dual acting compounds targeting aromatase and estrogen receptor α as an emerging therapeutic opportunity to counteract estrogen responsive breast cancer

Jessica Caciolla,[a,#] Silvia Martini,[b,#] Angelo Spinello,[c] Matic Pavlin,[c,d] Eleonora Turrini,[e] Federica Simonelli,[c] Federica Belluti,[a] Angela Rampa,[a] Alessandra Bisi,[a] Carmela Fimognari,[e] Nadia Zaffaroni,[b] Silvia Gobbi,[a,*] Alessandra Magistrato[c,*]

[a]Department of Pharmacy and Biotechnology, Alma Mater Studiorum-University of Bologna, via Belmeloro 6, 40126, Bologna, Italy

[b]Fondazione IRCSS Istituto Nazionale dei Tumori, via Amadeo 42, 20113, Milano, Italy

[c]National Research Council of Italy Institute of Materials (CNR-IOM) c/o SISSA, via Bonomea 265, 34136, Trieste, Italy

[d]Laboratory of Microsensor Structures and Electronics, Faculty of Electrical Engineering, University of Ljubljana, Tržaška cesta 25, SI-1000 Ljubljana, Slovenia

[e]Department for Life Quality Studies, Alma Mater Studiorum-University of Bologna, corso d'Augusto 237, 47921, Rimini, Italy

[#] These authors equally contributed to this manuscript

*Corresponding authors. E-mail addresses: silvia.gobbi@unibo.it (S. Gobbi), alessandra.magistrato@sissa.it (A. Magistrato)

Abbreviations: AI, aromatase inhibitor; AR, aromatase; BC, breast cancer; E2, estradiol; END, endoxifen; ER, estrogen receptor; ER+, estrogen receptor positive; ICI (182,780), fulvestrant; LBC, ligand binding cavity; LBD, ligand binding domain; MD, molecular dynamics; PGR, progesterone receptor; QM/MM, quantum mechanics/molecular mechanics; SERD, selective estrogen receptor degraders; SERM, selective estrogen receptor modulators; TAM, tamoxifen; ΔG_b, binding free energy.

Abstract

Breast Cancer (BC) is a leading cause of death in women, currently affecting 13% of female population worldwide. First-line clinical treatments against Estrogen Receptor positive (ER+) BC rely on suppressing estrogen production, by inhibiting the aromatase (AR) enzyme, or on blocking estrogen-dependent pro-oncogenic signaling, by targeting Estrogen Receptor (ER) α with selective Modulators/Degraders (SERMs/SERDs). The development of dual acting molecules targeting AR and ERα represents a tantalizing alternative strategy to fight ER+ BC, reducing the incidence of adverse effects and resistance onset that limit the effectiveness of these gold-standard therapies.

Here, *in silico* design, synthesis, biological evaluation and an atomic-level characterization of the binding and inhibition mechanism of twelve structurally related drug-candidates enable the discovery of multiple compounds active on both AR and ERα in the sub-μM range. The best drug-candidate **3a** displayed a balanced low-nanomolar IC_{50} towards the two targets, SERM activity and moderate selectivity towards a BC cell line. Moreover, most of the studied compounds reduced ERα levels, suggesting a potential SERD activity. This study dissects the key structural traits needed to obtain optimal dual acting drug-candidates, showing that multitarget compounds may be a viable therapeutic option to counteract ER+ BC.

Keywords: breast cancer, multitarget, aromatase inhibitors, SERM, SERD, molecular dynamics, QM/MM.

1. INTRODUCTION

Breast cancer (BC) is the most common malignant tumor and the second leading cause of cancer-related death in women [1]. According to Brest Cancer Fact and Figures 2019-2020, it is estimated that 13 % of women will develop an invasive BC in their lifetime [2]. A high percentage of BC (around 80%) is estrogen dependent and needs hormones to grow and proliferate [3].

Key enzyme in the biosynthesis of estrogens is aromatase (AR), a member of the cytochrome P450 superfamily [4], expressed in ovaries and in many other tissues, responsible for peripheral estrogens production in postmenopausal women [5]. Upon binding to the Estrogen Receptor (ER) α ligand binding domain (LBD), estrogens trigger a conformational change of its helix (H)12, inducing the formation of an ERα homodimer, which then binds DNA and control gene expression [6, 7].

Two main strategies are currently employed in the clinics to treat hormone-dependent BC patients: (i) preventing estrogens biosynthesis by inhibiting AR or (ii) modulating ERα activity with Selective Estrogen Receptor Modulators or Degraders (SERMs/SERDs). The third-generation Aromatase Inhibitors (AIs) exemestane, letrozole and anastrozole are highly specific and characterized by fewer side effects when compared to previous reported agents. AIs are also classified as steroidal (exemestane) and non-steroidal derivatives (anastrozole and letrozole), exhibiting a different inhibition mechanism: exemestane binds irreversibly to AR, acting as a suicide inhibitor, while anastrozole and letrozole are reversible and competitive inhibitors [8, 9], supposedly able to form a coordination bond between their azole moiety and the heme iron atom of AR [10]. Nevertheless, no experimental structural data are currently available to ensure their binding mode, which has been recently questioned [11, 12]. The inhibition of AR leads to estrogens depletion in the whole body, thus inducing significant adverse side effects, such as musculoskeletal disorders, arthralgia, increase of osteoporosis and fractures, and cardiovascular events [13-15].

SERMs bind to ERα inducing opposite activity in different tissues. They act as agonists, mimicking estrogens activity in bones and heart tissues, while acting as antagonists in breast tissue [16] and, depending on the profile of each drug, they are widely used for the treatment/prevention of BC (and other cancers) and osteoporosis. The most representative and currently used SERM for BC treatment is tamoxifen (*Z*-1-{4-[2-(dimethylamino)ethoxy]phenyl}-1,2-diphenyl-1-butene, TAM, Figure 1). Despite its clinical usefulness, TAM exerts significant side effects, the most important being the increased risk of endometrial cancer, due to its agonist activity in uterine cells, and thromboembolic events [17]. Additionally, the prolonged use of TAM leads to the possible development of intrinsic or acquired drug resistance [18]. Besides, its wide biological profile also includes antifungal, antioxidant, and antiviral activities, antiangiogenesis and apoptosis induction properties. Pharmacological studies have shown that TAM is a prodrug, and its anticancer activity is due to its active metabolites, the most abundant and active being endoxifen (END, Figure 1) [19].

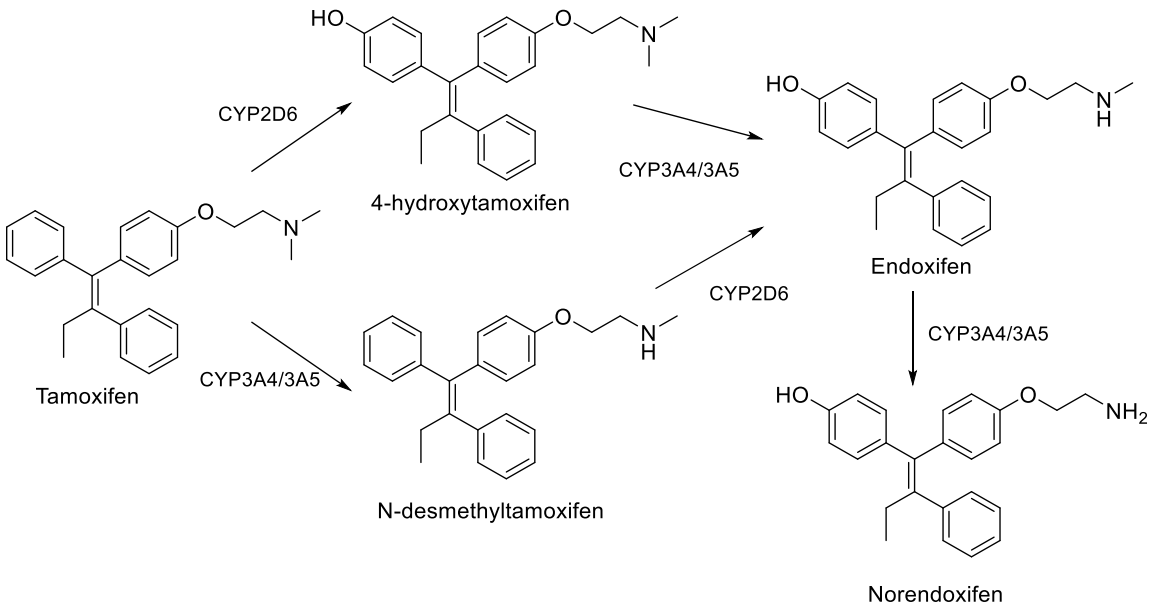

Figure 1. The most representative Selective Estrogen Receptor Modulator (SERM) tamoxifen (TAM) and its main metabolites.

Alternatively, SERDs have been developed, which bind to ERα triggering its degradation. Unlike SERMs, the interaction of SERDs with H12 of ER leads to alterations in its conformation and disruption of its structure, exposing different hydrophobic aminoacid residues, thus causing the ubiquitination and subsequent proteasomal degradation of the receptor. The prototype SERD, fulvestrant (ICI 182,780), although being a pure antagonist, exhibits poor pharmacokinetic properties, requiring intravenous administration and resulting in limited efficacy. Intense research efforts have been recently devoted to the discovery of SERDs that could counteract the resistance to prolonged therapeutic regiments due to the onset of somatic mutations in the LBD of ERα [20-22]. Although fulvestrant and AZD-9496, currently in phase I clinical trials [23], retain efficacy against the most diffused and aggressive ERα isoforms, alternative therapeutic strategies are urgently needed.

In principle, AI and SERM/SERD may act synergistically to inhibit the growth and proliferation of BC cells, leading to an increased efficacy when used in a combined treatment. Nevertheless, conflicting evidence emerged in distinct clinical studies. While Brodie and coworkers observed that the combination of letrozole and fulvestrant was more effective than the two drugs administered singularly [24], the ATAC (anastrozole, tamoxifen, alone or in combination) trial showed, instead, that anastrozole alone was more effective in terms of disease-free survival and time to recurrence when compared to TAM alone or to anastrozole and TAM in combination [25, 26]. As a result, an efficacy boost is not warrantied for any SERM and AI combination.

Among the novel strategies recently perused to counteract ER+ BC is the development of compounds with dual AI/SERM activity, able to simultaneously block estrogen production and ERα-mediated cell proliferation in BC tissues. Additionally, these dual acting agents may be endowed with fewer side effects, since the agonistic activity of SERM-like compounds in bone-tissue would alleviate the typical disturbances caused by AI-induced estrogen depletion, while the reduction of estrogen biosynthesis may counteract the agonist effects of SERM-like molecules on uterine tissue.

In this context, in 2012 Flockhart and coworkers reported that some TAM metabolites, namely END, N-desmethyltamoxifen and norendoxifen, act as AIs (K_i values of 4.0 μM, 15.9 μM and 35 nM, respectively), while still binding with good affinity to ERα [27, 28]. Strikingly, these molecules, simultaneously blocking the activity of two distinct targets involved in ER+ BC, laid the foundations for developing dual AI/SERM lead compounds. Recently, the structures of the aforementioned TAM metabolites were subjected to different chemical modifications, among which the removal of the amino side chain of SERMs and its substitution by a hydroxyl group, resulting into a symmetrical bisphenol structure [29]. TAM bisphenol, another known metabolite of this drug (Figure 2) had also been previously shown to possess significant affinity for ERs [30], supporting the hypothesis that the removal of the side chain did not affect the antiestrogenic activity of this class of compounds. Moreover, different nitrogen-containing moieties were also inserted on the ethyl group to coordinate the heme iron of the AR enzyme, mimicking the letrozole/anastrozole metal coordinating moiety. As an example, the introduction of an imidazole ring led to a potent and effective compound (**A**, Figure 2). Nevertheless, no dual-acting drug-candidate has so far been object of preclinical studies, thus calling attention to this burgeoning research field.

Inspired by these promising results, and taking advantage of our long-lasting experience in developing AIs and TAM-related compounds [31-34], here we designed different series of potential multitarget agents (Figure 2), to gain new insight on TAM-derived molecules.

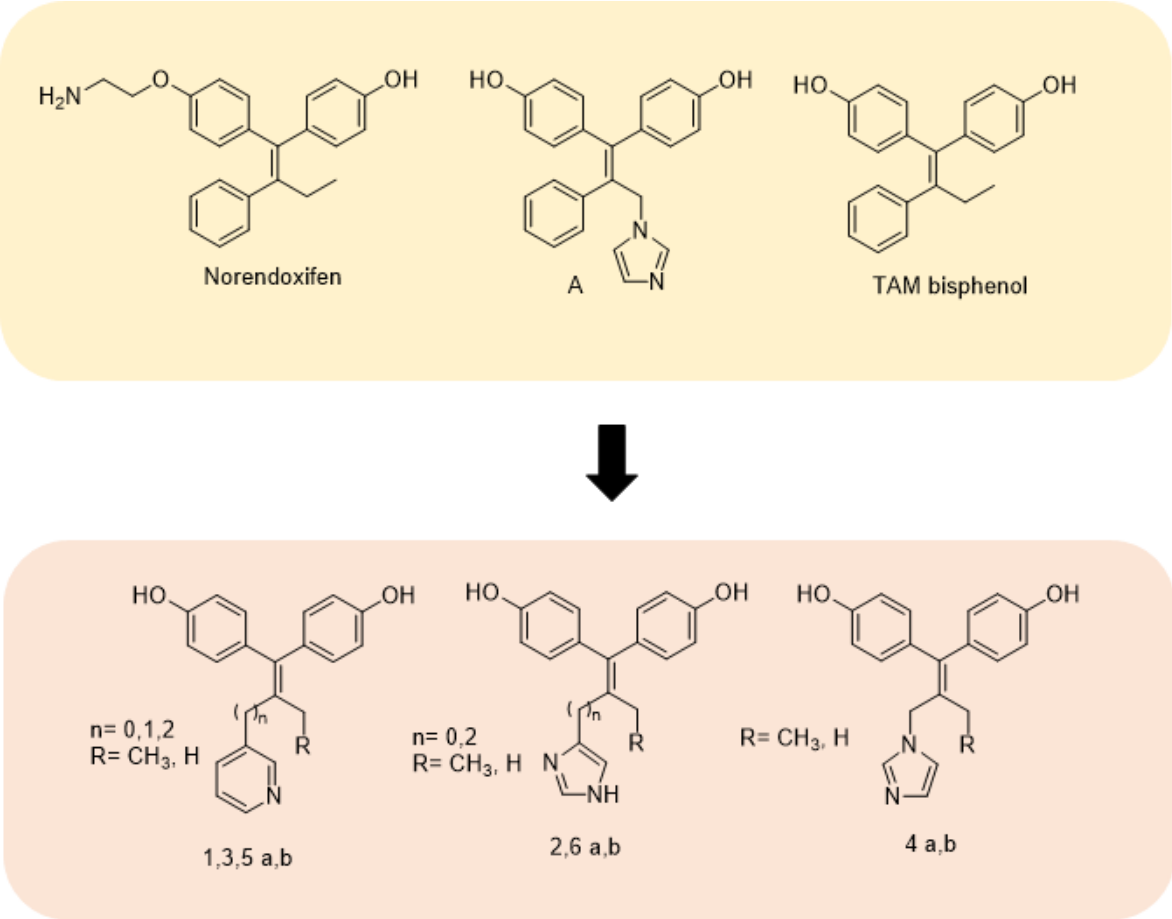

Figure 2. Design of the studied compounds.

After validating the aptitude of the designed ligands to fit into AR active site and ERα LBC, the compounds were synthesized and tested *in vitro* in order to evaluate their ability to inhibit AR and bind to ERα, their growth inhibition potency in BC and healthy breast cell lines, and their potential SERM and/or SERD effects. All-atom molecular dynamics (MD) simulations finally dissected the key structural traits underlying the striking inhibitory potency of the newly synthesized drugs-candidates.

2. RESULTS

2.1. Design and synthesis.

Building on the successful realization of other dual acting compounds [29], we conceived **1-6a,b** drug-candidates (Figure 2) on the basis of their potential ability to coordinate the heme moiety of AR, their structural similarity to TAM metabolites, and their synthetic feasibility.

In particular, the ethyl moiety, a distinctive feature of triphenylethylene SERMs, was maintained, and the key nitrogen atom, believed to establish a coordination bond with the heme iron of AR, was positioned in the existing aromatic ring, by substituting benzene with a pyridine or imidazole. A small spacer (1-2 carbon atoms) was also introduced between the nitrogen-containing moiety and the double bond, as in the literature molecule **A**, to evaluate the effect of its length on the activity, and the shortening of the ethyl chain to a methyl one was also explored. For these compounds docking simulations were performed to assess their ability to bind to the active site of AR and to the LBC of ERα.

Due to the well-known flaws of the docking simulations to reproduce the coordination bonds to the heme iron of AR, we imposed a constraint on the distance between the imidazole/nitrogen and the iron [35]. As a result, all ligands snugly fit within the AR active site with good docking scores (Table S1), but it is unclear if/unlikely that some of the compounds (**1a**, **1b**, **2a** and **2b**) would establish a coordination bond to the iron atom (Figure S1) owing to the lack of a spacer between the nitrogen-containing moiety and the double bond. As well, the twelve ligands were docked on a representative structure of the ERα LBD as obtained from previous classical MD simulations [6]. All ligands revealed good docking scores (ranging from -8 to -11 kcal/mol, Table S1), similarly to those predicted for END. On the basis of these results, we performed the synthesis of these ligands.

For the synthesis of compounds **1-3a,b** and **5-6a,b** (Scheme 1), 4,4'-dihydroxybenzophenone and the appropriate ketone (**7-11a,b**) were reacted under the McMurry reaction conditions, namely in the presence of titanium chloride and zinc powder to form a carbon-carbon double bond.

Scheme 1. Synthesis of compounds **1-3**, **5, 6**.[a]

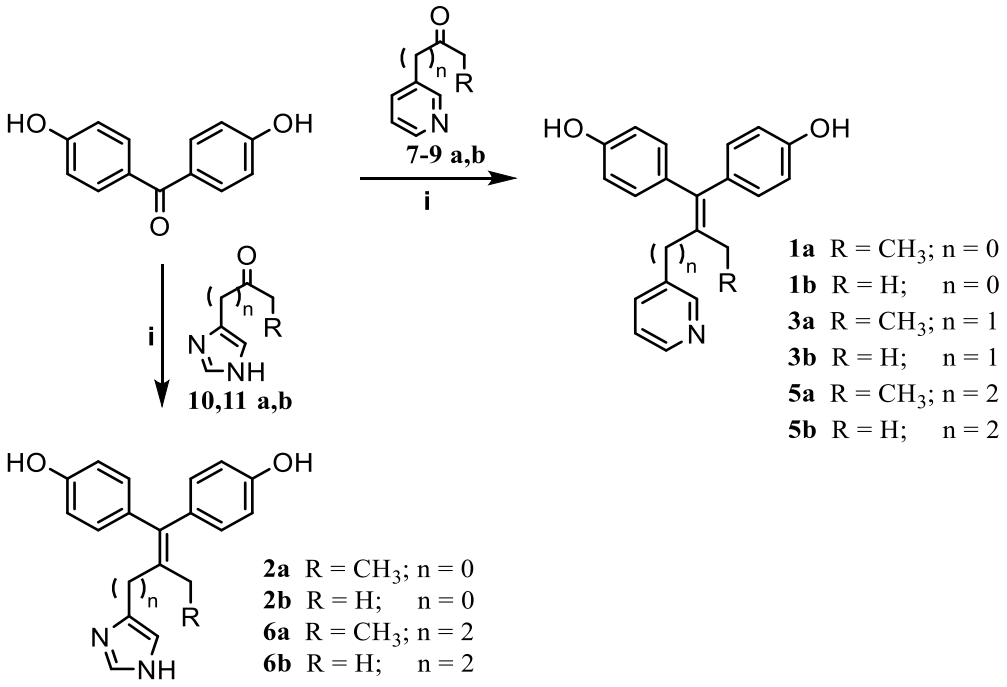

[a]**Reagents and conditions:** i) Zn, $TiCl_4$, THF, N_2, reflux, 3-5 h.

For the synthesis of compounds **4a,b** (Scheme 2), 4,4'-dihydroxybenzophenone and acetone or methylethylketone were reacted in the McMurry reaction to give **12a,b**. The hydroxyl groups were protected with chloromethylmethylether (MOM-Cl) and the obtained intermediates **13a,b** were first brominated with N-bromosuccinimide (NBS) and then reacted with imidazole to give **14a,b**. Cleavage of MOM ethereal functions, to obtain the free hydroxyl groups, by acid hydrolysis afforded compounds **4a** and **4b**.

Scheme 2. Synthesis of compounds **4a,b**.[a]

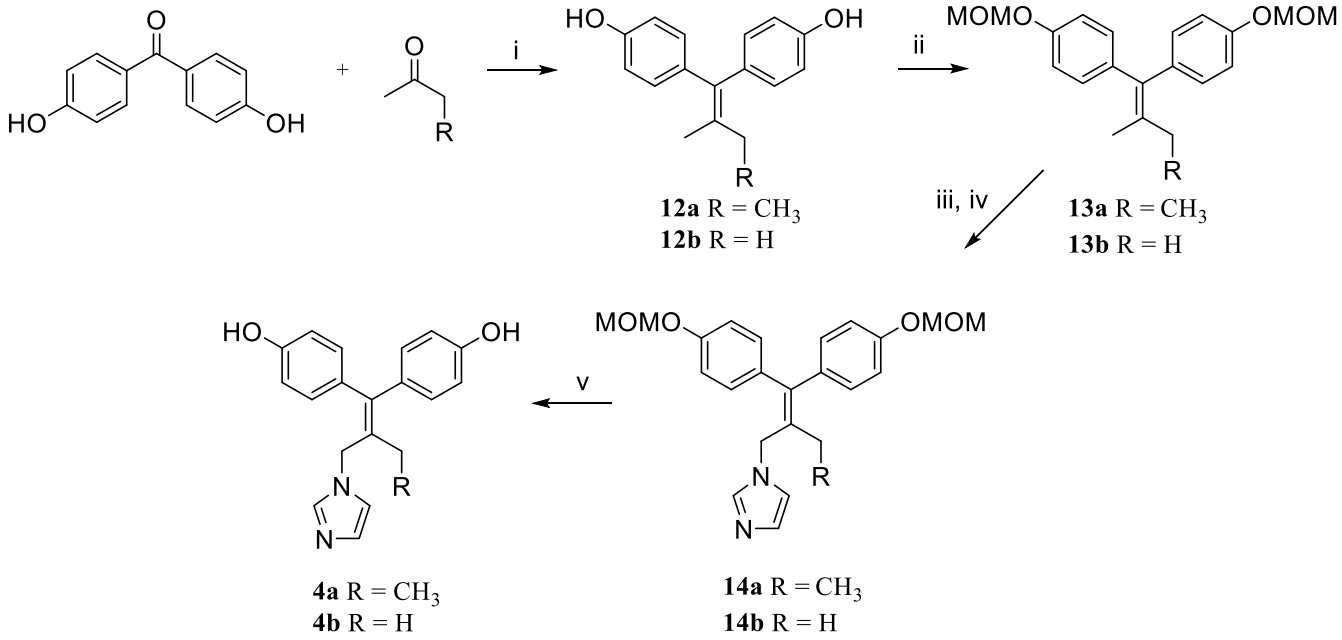

[a]**Reagents and conditions:** i) Zn, $TiCl_4$, THF, N_2, reflux, 3 h; ii) NaH 60 %, THF, MOM-Cl, N_2, r.t., 3 h; iii) NBS, CCl_4, BPO, hν, reflux 4 h; iv) imidazole, CH_3CN, N_2, reflux, 5 h; v) methanol, HCl, r.t., 12 h.

While the ketone intermediates **7a,b** and **8b**, for the synthesis of compounds **1a,b** and **3b** respectively, were commercially available, the other intermediates (**8a**, **9-11a,b)** were synthesized following different strategies (Schemes S1-S3).

2.2. *In vitro* assays of the synthesized compounds

The compounds were tested at different concentrations (from 0.0001 to 10 μM) for their ability to inhibit estrogen production by AR, by monitoring the conversion of a fluorogenic substrate of the enzyme into a highly fluorescent metabolite (Aromatase Inhibitor Screening Kit, BioVision) and results were reported in Table 1. For comparison letrozole was also tested as reference inhibitor. All compounds, except for **1b**, proved to be effective AIs and, remarkably, several ligands exhibited IC_{50} in the nM range. Overall, the obtained results suggested that the presence of the TAM-like ethyl moiety seemed to be preferred to the shorter methyl. As well, the introduction of either imidazole or pyridine led to potent derivatives, providing appropriate interactions of the designed molecules with AR.

In detail, the role and contribution of the heterocycle seemed to be dependent on the length of the spacer between the azole ring and the double bond. Indeed, apart from the weak AIs **1-2a,b,** bearing no linker (n = 0) and giving dissimilar results, both heterocycles led to equipotent compounds when separated from the vinyl moiety by a single-methylene spacer (n = 1, **3-4a,b**). Instead, imidazole seemed to be preferred to pyridine in the ethyl-linker derivatives (n = 2, **5-6a,b**).

Taking into account the data for the pyridine series, the introduction of a methylene between the azole ring and the double bond significantly boosted the activity of the compounds (**3a,b**), while its extension to two methylene units (**5a,b**) induced a decrease. As regards imidazole derivatives, the low micromolar activity of **2a**, carrying an ethyl moiety on the double bond, increased with the insertion of the methylene

spacer (n = 1, **4a**, IC_{50} = 35 nM), and was not affected by its lengthening (n = 2, **6a**). In contrast, the activity of the corresponding methyl derivatives was slightly reduced going from **2b** to **4b** (n = 1), but was remarkably improved by elongating the linker to two methylene units (n = 2, **6b,** IC_{50} = 63 nM). Altogether, among the synthesized compounds, **3a**, **4a**, **6a** and **6b** resulted to be the most potent AIs (IC_{50}s of 23, 35, 52 and 63 nM, respectively), exhibiting a slightly lower potency with respect to the reference inhibitor letrozole. Conversely, END had an IC_{50} > 10 μM.

The relative affinity of the new compounds and of the most active TAM metabolite END towards ERα (Table 1) was then evaluated using the PolarScreen ERα Competitor Assay Kit Green (Invitrogen) by measuring their ability to prevent estrogen binding to ERα. Apart from **1a**, all tested compounds were able to bind and displace the estrogen from ERα, showing IC_{50} values in the μM- or sub-μM range. From these results it clearly appeared that, except for **1-2a,b**, the introduction of a pyridine ring led in general to higher affinity for ERα as compared to imidazole, and that the TAM-like ethyl was preferred to the methyl moiety. Taking into account the activity of compounds bearing the ethyl group, in the pyridine series only the insertion of a methylene spacer on compound **1a** allowed a significant affinity gain for the receptor (**3a**, IC_{50} = 19 nM), while the elongation of the linker (**5a**, IC_{50} = 33 nM) did not further influence it. Concerning the corresponding imidazolyl derivatives, going from **2a** to **4a** a low activity was maintained, which was, instead, boosted by the insertion of another methylene unit (**6a**). Thus, the linker length had a lower impact on the measured IC_{50} in the pyridine series than in the corresponding imidazole group. Remarkably, only among compounds with no linker (**1-2a,b**), the presence of the methyl group on the double bond, rather than the ethyl, led to sub-μM affinity towards ERα, regardless of the choice of the heterocycle, being **1b** the most active derivative (IC_{50} = 76 nM). Compounds **3a** and **5a**, both carrying a pyridine ring and the ethyl group on the double bond, and a one- or two-methylene spacer, respectively, resulted to be the most interesting compounds, exhibiting IC_{50} comparable (**5a**) or lower (**3a**) than the reference END. Conversely, letrozole had an IC_{50} > 10 μM.

Moreover, we evaluated the ability of these compounds to inhibit the growth of the MCF-7 ER+ BC cell line and – for comparative purpose – that of a healthy breast cell line (MCF10A) (Table 1). Several molecules showed a moderate capability to inhibit cell growth in MCF-7 cells with IC_{50} values > 10 μM. Interestingly, almost all compounds required slightly higher concentrations to inhibit MCF10A healthy breast cells proliferation, suggesting a mild non-specific antiproliferative effect on cancer cells. Notably **2a**, **2b**, **3a** and **6a** had no effect on healthy cells at any concentration tested. Remarkably, the antiproliferative activity of previously reported dual acting AR/ERα drug candidates was not measured [29].

Table 1. Biological profiles of **1-6a**, **b**: compound concentrations inhibiting by 50% AR activity, ERα binding and the proliferation of MCF7 (ER+) BC cells and MCF10A healthy breast cells. A comparison with letrozole (LET) and endoxifen (END) as reference inhibitors for AR and ERα, respectively.

Compound	Code	AR inhibition[a] IC_{50} μM	ERα binding[a] IC_{50} μM	MCF-7 cells[a] IC_{50} μM	MCF-10a cells[a] IC_{50} μM

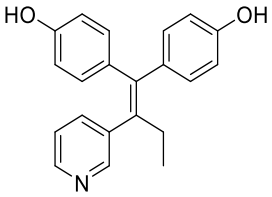	**1a**	1.253 ± 0.129	> 10	10.0 ± 2.1	17.0 ± 0.5
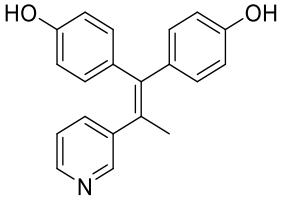	**1b**	> 10	0.076 ± 0.036	5.3 ± 1.1	41.7 ± 0.3
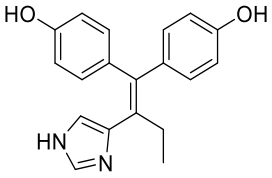	**2a**	0.952 ± 0.078	1.073 ± 1.010	60.0 ± 0.9	>100
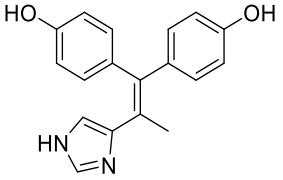	**2b**	0.596 ± 0.045	0.223 ± 0.071	58.0 ± 8.5	>100
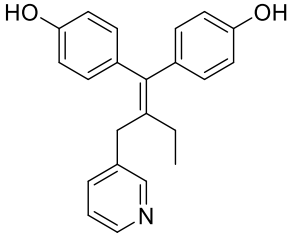	**3a**	0.023 ± 0.018	0.019 ± 0.001	27.6 ± 0.4	>100
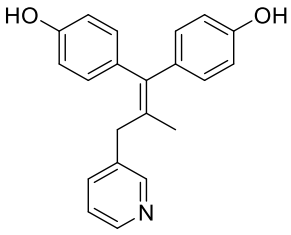	**3b**	0.861 ± 0.062	1.770 ± 0.368	41.2 ± 1.6	58.7 ± 0.9
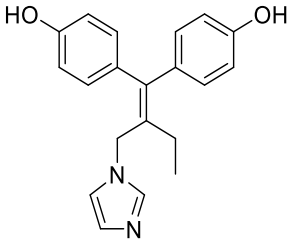	**4a**	0.035 ± 0.001	1.803 ± 0.221	24.3 ± 0.9	34.7 ± 0.5

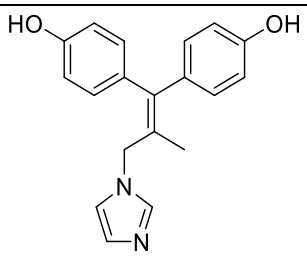	**4b**	1.002 ± 0.171	4.950 ± 0.613	37.0 ± 1.0	52.5 ± 0.5
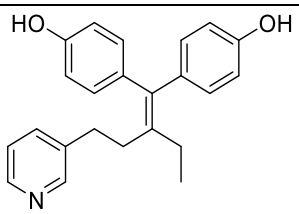	**5a**	0.900 ± 0.339	0.033 ± 0.003	42.1 ± 1.1	20.0 ± 1.6
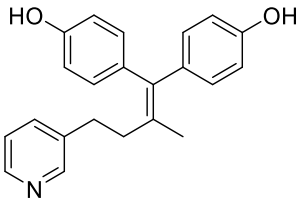	**5b**	3.240 ± 0.438	0.313 ± 0.006	>100	>100
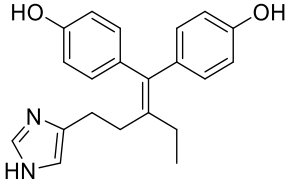	**6a**	0.052 ± 0.004	0.197 ± 0.031	37.1 ± 1.1	>100
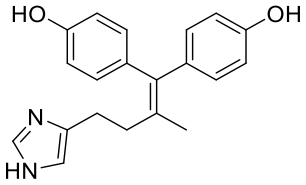	**6b**	0.063 ± 0.003	1.737 ± 0.318	39.8 ± 4.7	50.4 ± 0.7
Endoxifen		>10	0.030 ± 0.023	0.1 ± 0.1	>10
Letrozole		0.004 ± 0.001	>10	4.1 ± 1.1	>10

[a]Data represent the mean ± SD of at least three independent experiments performed in triplicate.

2.3. Analysis of progesterone receptor (PGR) mRNA expression in MCF-7 cells

A functional assay was then performed to assess the ability of two of the most promising compounds based on the above reported IC_{50}s, **3a** and **6a**, to antagonize the mRNA estrogen-stimulated expression of Progesterone Receptor (PGR) in MCF-7 cells [29]. Estradiol (E2) significantly increased the expression of PGR compared to untreated cells and E2-stimulated mRNA expression of PGR was considered 100%. The antiestrogenic activity of compounds **3a** and **6a** was then monitored as reduction of the aforementioned expression (Figure 3). END, used as positive control, antagonized the E2-stimulated mRNA expression of PGR to 5.6% (Figure 3), consistent with previously published results [36]. As well, **3a** and **6a** were able to dose-dependently antagonize the E2-stimulated expression of PGR, although to a weaker extent compared to the positive control END. Namely, they antagonized it up to 29

and 28%, respectively, at the highest tested concentration (20 µM) (Figure 3). These values are in line with those observed for previously reported dual-acting AR/ERα compounds [29].

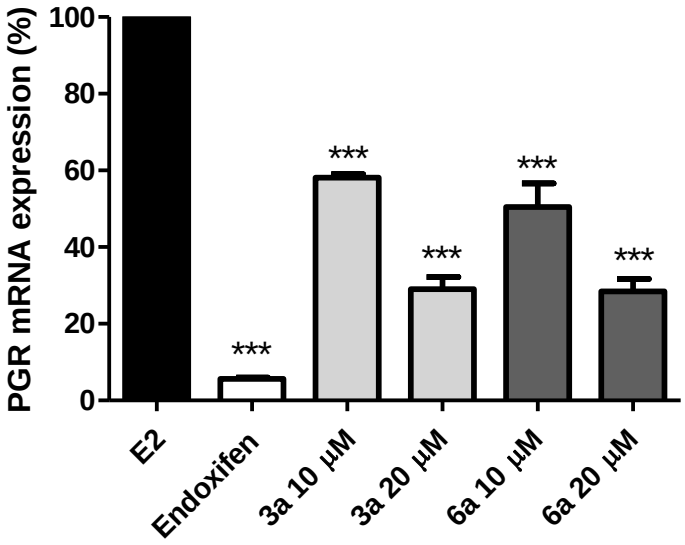

Figure 3. PGR mRNA expression level after treatment of MCF-7 cells with E2 (10 nM) alone (considered as 100% PGR mRNA expression) or E2 in association with compounds **3a** or **6a** (10-20 µM) or endoxifen (1 µM), used as positive control for its ability to antagonize stimulated PGR expression. ***$p < 0.001$ versus E2-stimulated mRNA expression of PGR.

2.4. Assessment of ERα expression in MCF-7 cells

Besides the capacity to prevent the binding of estrogen to ERα, crucial property of SERDs is the ability to degrade the receptor. To evaluate the efficiency of the studied molecules as potential multipotent agents, as a preliminary assay the ability of the compounds to modulate the expression of ERα was evaluated by Western Blot analysis, together with fulvestrant (ICI) as positive control. Based on the results of ERα binding assay, all compounds, except for **1a** ($IC_{50} > 10$ µM), were used at their specific IC_{50} calculated with the cell-free assay. Fulvestrant was used at a fixed concentration of 1 µM.

As shown in Figure 4, a reduction of protein levels, although to a different extent, was obtained with the tested compounds, with the exception of **2a**, **3b**, **4b** and **6b**. Compounds **2b**, **4a** and **5a**, with IC_{50}s of 223 nM, 1800 nM and 33 nM, respectively, showed excellent activity on ERα degradation. Similar to fulvestrant, compound **5b** almost completely degraded ERα, but at a lower concentration (313 nM vs 1.0 µM). Interestingly, compound **3a**, which showed the highest binding affinity towards ERα in the binding assay ($IC_{50} = 19$ nM), also demonstrated an outstanding degradation activity against ERα in MCF-7 cells, as shown in Figure 4.

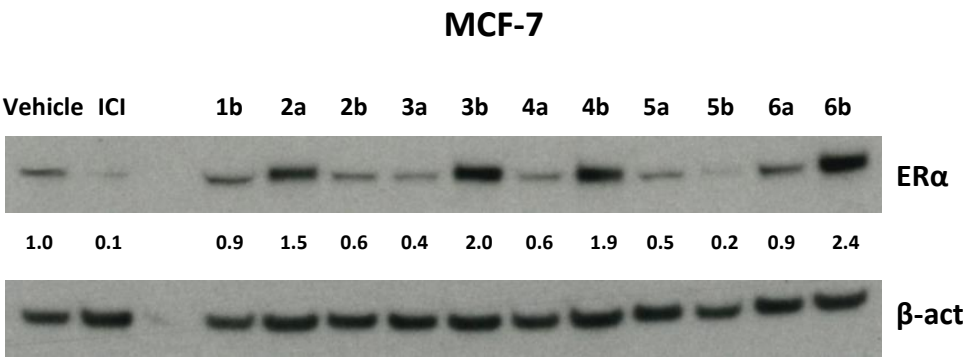

Figure 4. Representative western blotting showing the expression of ERα in MCF-7 cells exposed to vehicle (DMSO) or to the studied compounds (IC_{50} calculated by ERα binding assay) and fulvestrant (ICI, 1 μM). β-actin was used to confirm equal protein loading on the gel. For each protein, band density was quantified using ImageJ [37] normalized to loading control and referred to untreated control.

2.5. Molecular mechanism of inhibition

Aiming to exhaustively dissect the structural traits underlying the experimentally measured efficacy of the synthesized compounds, we performed extensive force field-based MD and mixed quantum-classical (QM/MM) MD simulations. These allowed to predict the inhibitors binding mode to AR and to the LBD of ERα and to identify the key interactions they established with both target biomolecules.

Consistently with previous studies [35], the docking scores of the inhibitors on AR do not correlate with the measured IC_{50}, owing to the inability of the docking simulations to describe coordination bonds. Thus, in order to understand which drug may owe its potency to a coordination bond to the iron atom, we performed QM/MM MD simulations to accurately account for the metal-ligand interaction, while explicitly considering the biomolecular environment [38]. Due to the high computational cost of QM/MM MD simulations, we selected a subset of compounds (**3a**, **3b**, **4a**, **4b**, **5a**, **6a**, **6b**) to find a rationale between their structural motifs and measured IC_{50}s.

Each AR/drug adduct was initially relaxed by 100 ns of explicitly solvated classical MD simulations and its equilibrated structure underwent 10 ps of QM/MM MD simulations. In line with our previous study [35], a structural analysis of the resulting adducts clearly disclosed that the coordination geometry (*i.e.* bond lengths and angles) of the inhibitors was not strictly entwined with the observed potency. Indeed, the most potent compounds **3a**, **4a**, **6a** and **6b** presented a binding geometry similar to **4b**, which is, instead, characterized by lower inhibitory potency. As well, the clinically used letrozole exhibited even longer coordination bonds distances [35]. Strikingly, **3b** and **5a** in QM/MM MD trajectories do not establish any coordination bond to the heme iron (Table 2), confirming common intuition that the possibility of binding the metal moiety boost the inhibitory potency. The AR active site is small and rigid and adapts with difficulty to ligands of shape different from its endogenous substrate. For this reason, even small differences among distinct inhibitors can strongly affect the binding properties. As an example, in the case of compound **5a**, the simultaneous presence of a two-methylene unit spacer, connecting the vinyl moiety to the pyridine, and of an ethyl substituent made the ligand very bulky, preventing the formation of a coordination bond (Figure 5). Conversely, from the docking poses of **2a** and **2b**, (Figure S1) it appeared that the absence of a methylene linker between the double bond and the

heterocycle made the latter highly rigid, due to the delocalization of the π−orbitals. This strikingly affected its ability to rotate and establish the coordination bond to the metal center.

Table 2. Structural characteristics for the binding of compounds **3a**, **3b**, **4a**, **4b**, **5a**, **6a**, **6b** to the active site of AR. The table reports the coordination bonds (Angstrom) and angles (deg) of the azole/pyridine moiety of the ligand to the heme iron atom. For comparison, the clinically used inhibitor letrozole (LTZ), having an IC_{50} of 4 nM, is also reported [11].

	Distance (Å)	**Angle (deg)**
LTZ	2.33 ± 0.15	91.8 ± 2.7
3a	2.27 ± 0.11	92.2 ± 6.7
3b	---	---
4a	2.16 ± 0.07	84.4 ± 7.8
4b	2.20 ± 0.11	89.6 ± 5.1
5a	---	---
6a	2.19 ± 0.08	95.0 ± 6.1
6b	2.20 ± 0.11	87.2 ± 4.7

We also monitored the role of the hydroxyl substituents in establishing hydrogen (H)-bonds to the active site residues. In spite of the similar coordination geometry, among the ligands predicted to coordinate the heme, the hydroxyl groups of **4a**, **6a** and **6b** established two persistent H-bonds to the backbones of Leu372 and Asp309, while **3a** H-bonded only to the backbone of Leu372 (Figure S2 and Table S2). Notably, also the clinically used inhibitors letrozole and exemestane can establish persistent H-bonds to the backbone of Met374 [35]. The presence of these H-bonds appeared therefore as another critical element to boost AI potency to the sub μM range.

In general, even the ligands unable to coordinate the iron atom, owing to geometric constraints, as **4b**, can engage a persistent H-bond with the backbone of Leu372, providing a rationale for their activity in the low μM range. In order to dissect the key interactions of inhibitors with the AR catalytic site, we also calculated their binding free energy (ΔG_b) with the Molecular Mechanics Generalized Born Surface Area (MM-GBSA) method [39]. Next, by performing a decomposition analysis, we picked the residues and the nature of the interactions that more strongly contribute to ΔG_b of each inhibitor. We remark that this type of analysis, performed at force field level on the QM/MM geometries, completely neglects the contribution of the inhibitor-Fe coordination bond and only provides information on classical non bonded interactions (hydrophobic or electrostatic interactions) between the ligand and the protein. Interestingly, the most potent inhibitors **3a**, **4a**, **6a** and **6b** established hydrophobic interactions between their ethyl moiety and Ile133 and Trp244, and between their phenol rings and Val370 and Leu372 (Table S3).

The analysis of predicted binding poses hence provided a structural explanation of previous SAR considerations, disclosing that an optimal spacer length, which enables the coordination to the heme coordinating moiety without making the substituent too bulky, and the ethyl group, which, instead, fills

the hydrophobic cavity, allow for a flexible inhibitor architecture adaptable to the tight structural constraints of the AR active site.

Next, we performed extensive classical MD simulations on the docking pose of each inhibitor/ERα adduct to provide a rationale for the activity of the compounds measured on ERα. For each of the 12 adducts we performed 500 ns of MD simulations.

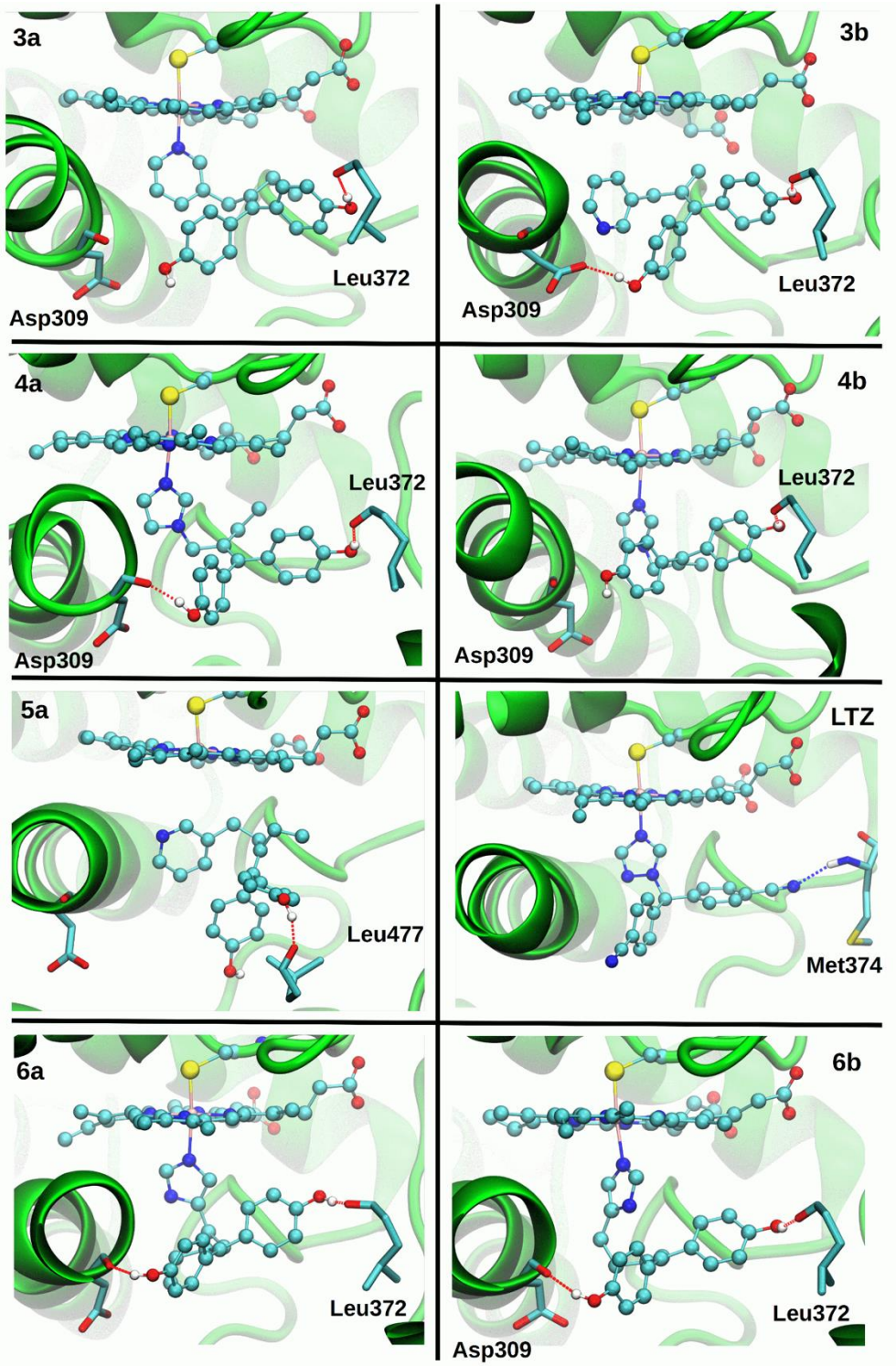

Figure 5. Binding pose of letrozole (LTZ) and the selected newly synthesized inhibitors **3a**, **3b**, **4a**, **4b**, **5a**, **6a** and **6b** to the aromatase (AR) active site as obtained from representative frames of QM/MM MD trajectories. AR structure is displayed in green new cartons, the heme moiety, the cysteine and the inhibitors are shown in balls and sticks, the residues forming hydrogen bonds to the ligands are shown in licorice. All atoms are coloured by atom name (H white, O red, S yellow and N blue, C cyan).

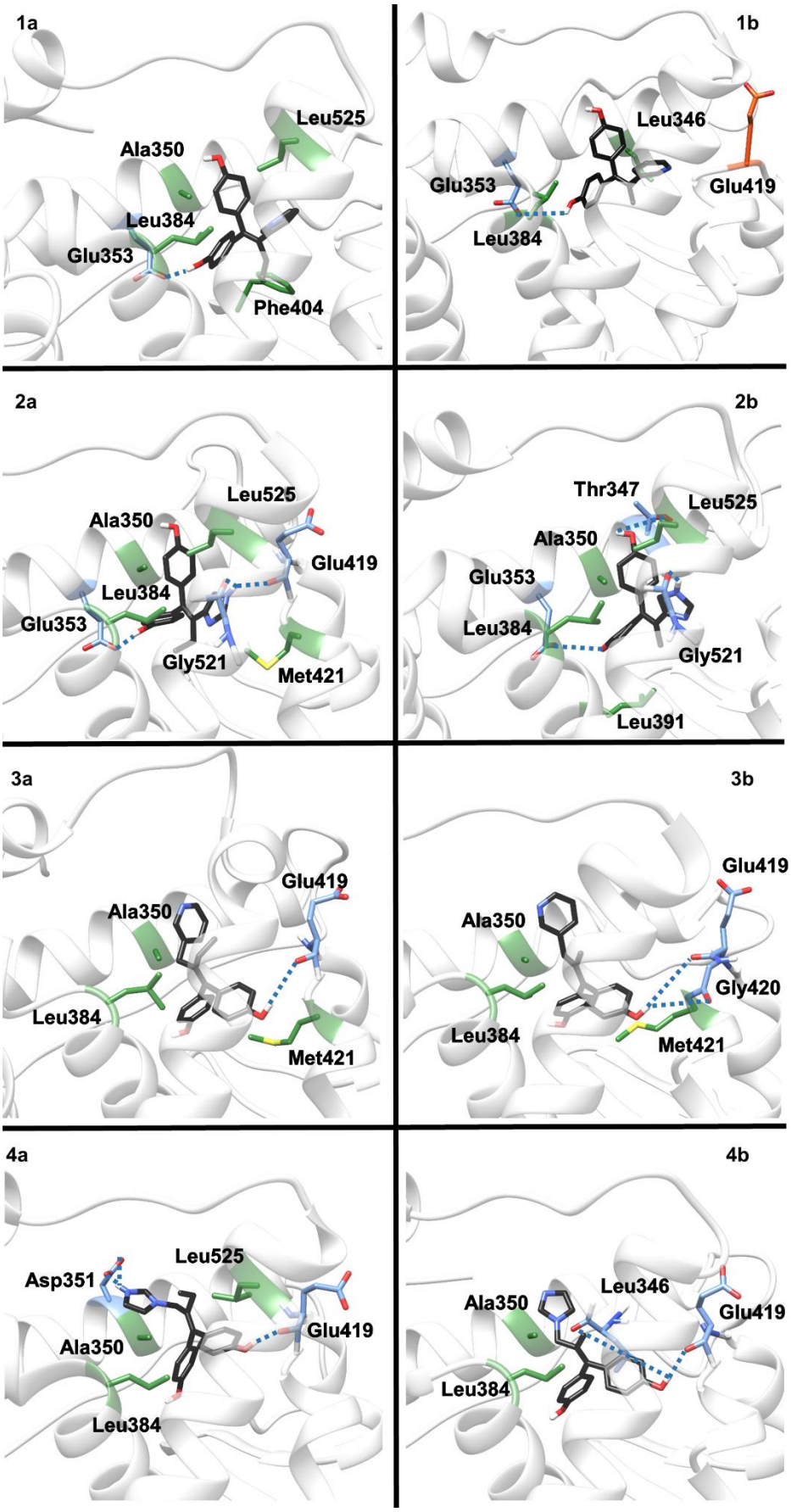
1a
Leu525
Ala350
Leu384
Glu353
Phe404
1b
Leu346
Glu353
Glu419
Leu384
2a
Leu525
Ala350
Glu419
Leu384
Glu353
Gly521
Met421
2b
Thr347
Leu525
Ala350
Glu353
Leu384
Gly521
Leu391
3a
Glu419
Ala350
Leu384
Met421
3b
Glu419
Ala350
Gly420
Leu384
Met421
4a
Leu525
Asp351
Glu419
Ala350
Leu384
4b
Leu346
Ala350
Glu419
Leu384

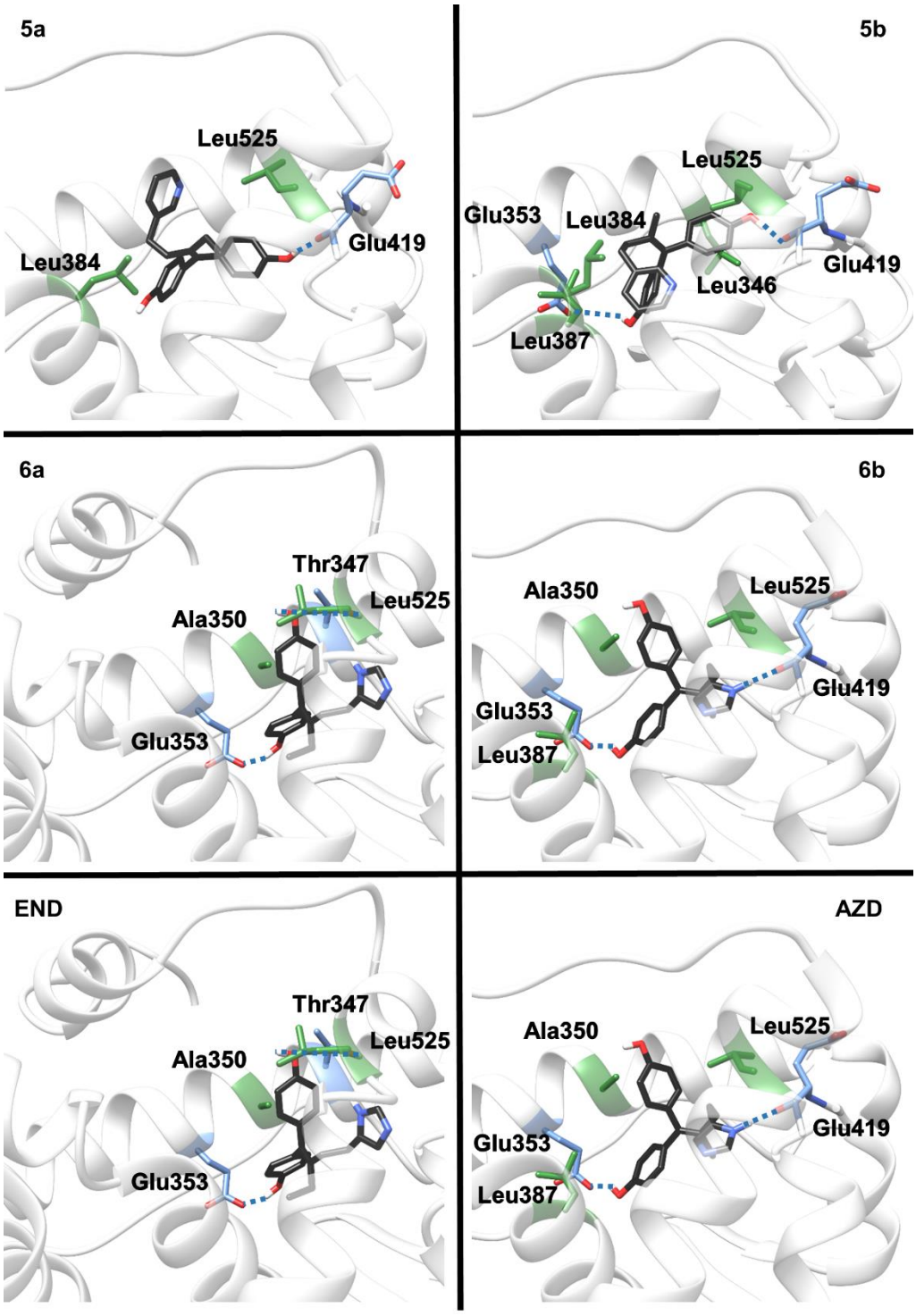

Figure 6. Binding pose of the synthesized inhibitors to the ligand-binding cavity of ERα as obtained from a representative cluster (Table S4) of classical MD trajectory. The binding mode of endoxifen (END) and AZD-9496 (AZD), are also reported for comparison. ERα is shown as white new cartoons, the drug is displayed with back carbon atoms, the residues forming hydrophobic interactions are shown in green, those forming hydrogen-bonds are shown in blue, residues disfavouring the binding (in the

decomposition energy analysis reported in Table S7) are displayed in orange. The rest of the atoms are coloured by atom name (H white, O red, S yellow and N blue).

Table 3. Total and Decomposition of the binding free energy (ΔG_b, kcal/mol) obtained from Molecular Mechanics Generalized Surface Area for the binding of **3a** to the aromatase (AR) enzyme (a) and to Estrogen receptor (ER) α (b) as obtained from this QM/MM and classical molecular dynamics trajectories analyses, respectively. The residues which contribute to ΔG_b by more than 0.5 kcal/mol are listed.

3a/AR ΔG_b tot= -15.95 ± 8.93	
Residue	ΔG_b per residue
Arg115	-0.86 ± 0.66
Ile133	-1.21 ± 0.41
Phe134	-0.80 ± 0.20
Trp224	-1.52 ± 0.31
Ala306	-0.64 ± 0.45
Asp309	-0.71 ± 0.40
Thr310	-0.93 ± 0.52
Val370	-1.92 ± 0.32
Leu372	-1.54 ± 0.57
Val373	-0.89 ± 0.28
Met374	-1.15 ± 0.35
Leu477	-1.18 ± 0.38
Ligand	-7.31 ± 4.36

(a)

3a/ERα		
	Monomer A **ΔG_btot= -37.50 ± 3.70**	**Monomer B** **ΔG_btot= -34.28 ± 2.54**
Residue	ΔG_b per res**idue**	ΔG_b per res**idue**
Met343		**-0.79 ± 0.29**
Leu346		**-1.19 ± 0.50**
Thr347		**-0.69 ± 0.24**
Leu349		**-0.92 ± 0.26**

Ala350	**-1.57 ± 0.44**	**-1.79 ± 0.30**
Trp383	**-0.74 ± 0.27**	
Leu384	**-1.93 ± 0.32**	**-1.11 ± 0.41**
Leu387	**-0.78 ± 0.31**	**-1.46 ± 0.63**
Met388	**-0.92 ± 0.40**	**-1.01 ± 0.32**
Leu391	**-0.86 ± 0.29**	**-1.16 ± 0.34**
Phe404	**-0.75 ± 0.24**	**-0.91 ± 0.27**
Val418	**-1.18 ± 0.43**	**-0.56 ± 0.24**
Glu419	**-0.74 ± 1.09**	
Met421	**-1.99 ± 0.52**	**-1.12 ± 0.27**
Ile424	**-0.56 ± 0.25**	**-0.63 ± 0.22**
Leu428		**-0.62 ± 0.21**
Met522	**-0.51 ± 0.14**	
Hie524	**-0.72 ± 0.51**	**-0.78 ± 0.37**
Leu525	**-1.43 ± 0.46**	**-3.47 ± 0.42**
Met528	**-1.49 ± 0.55**	
Ligand	**-17.84 ± 1.85**	**-14.90 ± 1.31**

(b)

Compounds **3a** and **5a** proved to be the most potent of the series, inhibiting estrogen binding to ERα with IC_{50} values of 19 and 33 nM, respectively. Strikingly, these molecules presented among the highest ΔG_b to ERα (Table S5), consistently with docking scores (Table S1). A decomposition analysis clearly revealed that their binding is stabilized by hydrophobic interactions (Figure S5 and Tables 3 and S5-S7). In particular, **3a** establishes hydrophobic interactions with Ala350, Leu384 and Met421 (Table S7) and H-bonds between the hydroxyl of one phenol ring to the backbone of Glu419 and His424 (Figure 6 and Table S8). As well, **5a** is mostly stabilized by hydrophobic interactions, being Leu346, Ala350, Leu384, Leu387, and Leu525 the residues mostly contributing to its ΔG_b. This latter ligand shares with **3a** the same persistent H-bond to the backbone of Glu419. Ostensibly, most compounds, irrespectively of their IC_{50}, often H-bond to Glu419 and/or Glu353 (Table S2) and are stabilized by a similar set of hydrophobic interactions of the most active inhibitors, pinpointing that the ΔG_b *per se* does not fully account for their measured IC_{50}.

In order to assess the impact of the inhibitors on the structural and dynamical properties of ERα, we also inspected how their binding affected the H-bond network of H12, which is known to trigger the conformational switch between the active and the inactive state of ERα. This H-bond network was previously pinpointed by us to a signature of ERα activation [6]. Consistently with our previous study, where END was observed to stabilize the antagonist conformation of ERα by preventing the formation of H-bonds between Glu380 and Tyr537 or the backbone of Leu536, **3a** and **5a**, characterized by the best IC_{50}, exhibited a reduced H-bond network around Glu380 with respect to the inhibitors endowed with lower activity.

The presence/absence of this H-bond network must translate in the presence/lack of specific cross correlation contacts (*i.e.* dynamically correlated motion) between H12 and H3/H5, underlying the activation of ERα [6]. Hence, we computed a coarse version of the cross-correlation matrix to monitor the dynamical coupling of the specific ERα structural elements (Figures 7 and S5, S6). Remarkably, all ligands exhibited small correlation coefficients between H12 and H3/H5, similarly to END, suggesting their binding stabilize the antagonist conformation of ERα (Figures 6 and S5), consistently with their activity as SERM/SERD compounds.

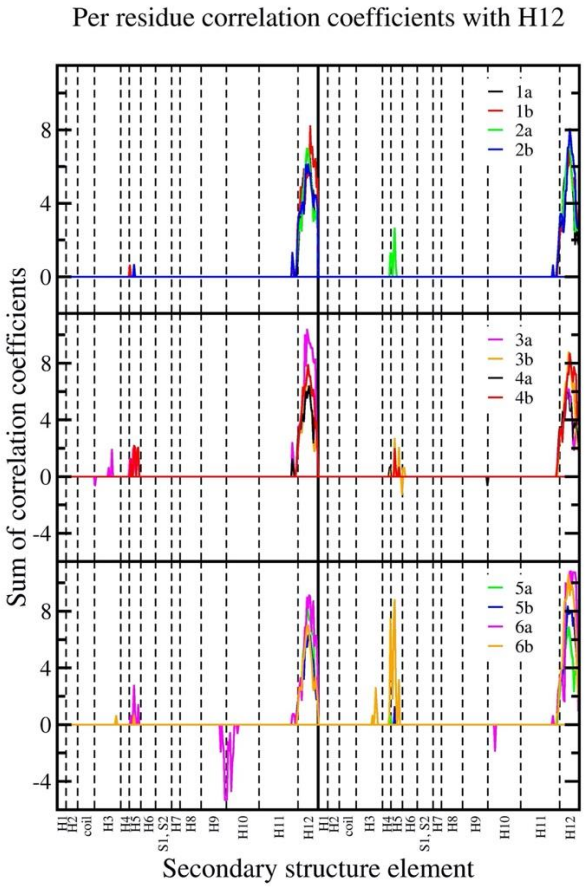

Figure 7. Sum of per-residue cross-correlation coefficients of H12 residues with the rest of the motifs composing Ligand Binding Domain (LBD). Left and right columns refer to monomers A and B, respectively. Top report the correlation coefficient of **1-6a,b** bound to ERα, bottom reports the internal

correlation of **1b** and **5a** to Y537S ERα. ERα LBD monomer structural motifs are labeled as, H1: residues 303–311; H2: residues 312–322; coil2–3 (C2–3): residues 323–338 (orange); H3: residues 339–363; H4: residues 364–371; H5: residues 372–382; H6: residues 383–396; S1, S2: residues 397–411; H7: residues 412–419; H8: residues 420–439; H9: residues 440–463; H10: residues 464–494; H11: residues 495–531; H12: residues 532–552. See Figure S6 for a visual map of the decomposition.

3. DISCUSSION

In this study, multitarget AI/ERα ligands were designed, synthesized, subjected to biological evaluation and structurally characterized, in order to generate drug-candidates that may offer improved efficacy and lower side effects compared to a single drug or a combination of AI and SERM/SERD.

Considering AR inhibition activity, the presence of the TAM-like ethyl group and a spacer between the double bond and the heterocycle appeared as critical hallmarks for high potency. In detail, for compounds carrying a pyridine ring, only the methylene spacer proved to have the optimal length for appropriately accommodating into AR active site. Conversely, for imidazole-based derivatives, the extension of the linker to two methylene units did not reduce the affinity for the target, leading to an equipotent activity of elongated compounds carrying a methyl (**6b**) and ethyl (**6a**) moiety on the double bond. Even though most of the compounds exhibiting the best IC_{50}s as AIs carried imidazole as heterocycle (**4a**, **6a** and **6b**), the most potent compound resulted to be **3a**, which, instead, contains a pyridine group. This evidence suggests that both heterocycles allowed for the appropriate interactions with AR, when a suitable and AR-adaptable structure of the whole molecule was provided, leading to the development of potent AIs.

Considering the affinity of the compounds towards ERα, the presence of a spacer, together with the TAM-like ethyl moiety, again seemed to be critical structural traits for optimal binding. Indeed, the most potent compounds (**3a** and **5a**, IC_{50}s of 19 nM and 33 nM, respectively) carried the ethyl moiety on the double bond, beside a pyridine ring and a spacer. As an exception, **1b** with no linker and a methyl substituent on the double bond, also proved to have high affinity. Nonetheless, no other clear SAR information could be gained, since similar sub-μM potency was seen for both rigid no-spacer molecules and flexible one- or two-methylene linker derivatives. This outcome may be due to the flexible nature of the receptor LBC, which adapts more easily than AR to the binding of the drug-candidates. Stunningly, the best performing compound presents a better IC_{50} than the reference END.

In view of developing novel multitargeting strategies, the most interesting result was the identification of compounds able to modulate both AR and ERα, in some cases, with significant and balanced potency. In particular, both **2b** and **6a** proved to be sub-μM AIs and ERα ligands, although their activities were not perfectly balanced. Most importantly, **3a** was endowed with a striking activity in the low nanomolar range (IC_{50}s of 23 (AR) and 19 (ERα) nM) on both targets, showing a moderate selective antiproliferative effects on a BC cell line. Notably, this compound showed a more balanced activity when compared to previously reported AR/ERα dual acting compounds.

The most interesting compounds identified, **3a** and **6a**, also proved to be endowed with SERM activity, being able to antagonize the expression of progesterone receptor. Notably, most of the studied compounds, displaying sub-μM IC_{50} towards ERα, reduced ERα levels to an extent comparable to that observed with fulvestrant. **5b** showed the most remarkable effect at a lower dose than the reference compound, and could be worth further evaluation to access its potential as a promising SERD candidate.

Given these results, **3a** proved to be the most promising and balanced dual acting AI-SERM candidate of the series, displaying a significant reduction of ERα protein amount and no cytotoxicity towards healthy mammary cells.

Remarkably, our detailed characterization provides a practical guideline of the key structural traits typifying a potent and balanced AR/ERα multitarget anti ER+ BC compound, such as the most potent and balanced compound **3a**: (i) the presence of the hydroxyl substituents enables the formation of a persistent H-bond to the backbone of Leu372 of AR, and to the backbone of Glu419 of ERα, (ii) the ethyl moiety fills both the active site of AR and the LBC of ERα, allowing in AR the formation of a coordination bond to the iron atom and of an optimal set of hydrophobic interactions in both targets. Remarkably the AR active site and the LBC of ERα share a highly similar content of hydrophobic residues (the residues present within 3 Å of **3a** are 3 Leu, 2 Val, 2 Phe, 1 Thr, 1 Met, 2 Trp, 1 Arg, for AR and 5 Leu, 1 Val,1 Thr, 3 Met, 1 Phe for ERα); (iii) the presence of a methylene linker, connecting the pyridine moiety to the vinyl core, enables an internal π-stacking, between the pyridine and the phenol ring in cis position on the double bond core, while hydrophobic interactions occur between the remaining ethyl and phenol moieties. This inhibitor's scaffold enables the formation of optimal interactions with the target cavity. In detail, the intramolecular π-stacking of the pyridine and the phenol extends to Trp224, which closes the AR active site, while Val370 is packed between the two inhibitor's phenol rings. Conversely in ERα, the pyridine/phenol are lined by Ala350 and Leu384 and two methionine residues (Met388 and Met421) insert between the phenols, while Leu525 and Met528 line the ethyl moiety of the ligand. Hence, a dual acting drug-candidate must be able to mainly establish hydrophobic interactions with the functional sites of the two targets, as well as intra-ligand hydrophobic interactions, which allow it to pack and snugly fit in the binding cavity.

In conclusion, this study provides novel potent, selective and balanced dual-targeting AR/ERα modulators as antitumor drug-candidates, unprecedentedly unveiling the potential of a pyridine substituent as a structural moiety to be employed in the development of novel multipotent anticancer agents. This study strongly remarks that the development of multipotent compounds, able to simultaneously modulate these utmost important BC targets, could represent an appealing and viable therapeutic strategy to expand the current arsenal of pharmacological strategies in the ever-harsher battle against BC.

4. EXPERIMENTAL SECTION

4.1. Chemistry.

4.1.1. General Methods. Starting materials, unless otherwise specified, were used as high grade purity commercial products. Solvents were of analytical grade. Reaction progress was followed by thin layer chromatography (TLC) on precoated silica gel plates (Merck Silica Gel 60 F254) and then visualized with a UV254 lamplight. Chromatographic separations were performed on silica gel columns by flash method (Kieselgel 40, 0.040-0.063 mm, Merck). Melting points were determined in open glass capillaries, using a Büchi apparatus and are uncorrected. ^{1}H NMR and ^{13}C NMR spectra were recorded on a Varian Gemini spectrometer 400 MHz and 101 MHz, respectively, in $CDCl_3$ solutions unless otherwise indicated, and chemical shifts (δ) were reported as parts per million (ppm) values relative to

tetramethylsilane (TMS) as internal standard; coupling constants (*J*) are reported in Hertz (Hz). Standard abbreviations indicating spin multiplicities are given as follow: s (singlet), d (doublet), t (triplet), br (broad), q (quartet) or m (multiplet). Mass spectra were recorded on Waters Xevo G2-XS QTof apparatus operating in electrospray mode (ES). All tested compounds were found to have >95% purity, as determined by HPLC analysis, performed on a chromatograph PU-1587 UV model equipped with a 20 µL loop valve (Jasco Europe, Italy) by using a Phenomenex Luna 5 µm C18 column (150 × 4.60 mm) as stationary phase and a mixture of H_2O/MeCN (60:40, v/v) as mobile phase for compounds **1a,b**, **3a,b** and **5a,b**, or a Waters Spherisorb 5 µm C18 column (250 x 4.60 mm) as stationary phase and a mixture of H_2O/MeCN (70:30, v/v) as mobile phase for compounds **2a,b**, **4a,b** and **6a,b**; for all compounds, detection at λ = 254 nm, flow rate of 1.0 mL/min. Compounds were named relying on the naming algorithm developed by CambridgeSoft Corporation and used in ChemDraw Professional 19.0.

4.1.2. General procedure of McMurry reaction.

Method A. Zinc powder (10 eq) was suspended in anhydrous THF, the mixture was cooled to 0 °C and $TiCl_4$ (5 eq) was added dropwise under nitrogen atmosphere. At the end of the addition, the mixture was brought to room temperature and then warmed to reflux for 2 hours. After cooling, a solution of benzophenone (1 eq) and the corresponding ketone (3 eq) in dry THF was added and the mixture was heated to reflux in the dark for 3 hours. After cooling, the mixture was poured into a 10 % K_2CO_3 solution and extracted with diethylether (3 x 25 mL). The combined organic layers were washed with brine, dried over anhydrous Na_2SO_4 and concentrated to dryness. The crude compound was then purified by flash column chromatography with a suitable eluent to provide the desired McMurry product.

Method B. Zinc powder (6 eq) was suspended in anhydrous THF, the mixture was cooled to 0 °C and $TiCl_4$ (3 eq) was added dropwise under nitrogen atmosphere. At the end of the addition, the mixture was brought to room temperature and then warmed to reflux for 1 hour. After cooling, a solution of benzophenone (1 eq) and the corresponding ketone (1 eq) in dry THF was added and the mixture was heated to reflux for 2 hours. After cooling, the mixture was poured into a 10 % K_2CO_3 solution and extracted with diethyl ether (3 x 25 mL). The combined organic layers were washed with brine, dried over anhydrous Na_2SO_4 and concentrated to dryness. The crude compound was then purified by flash column chromatography with a suitable eluent to provide the desired McMurry product.

4.1.2.1. 4,4'-(2-(pyridine-3-yl)but-1-ene-1,1-diyl)diphenol (1a). Bis(4-hydroxyphenyl)methanone (0.50 g, 2.30 mmol) and 1-(pyridin-3-yl)propan-1-one (**7a**) (0.29 mL, 2.30 mmol) in dry THF (11.80 mL) were reacted according to **Method B**. The crude was purified by flash column chromatography (petroleum ether/ethyl acetate 1:1) to give **1a** (0.18 g, yield 24 %), mp 240-241 °C. ^{1}H NMR (methanol-*d*$_4$): δ 0.95 (t, *J* = 7.4 Hz, 3H, CH_3), 2.55 (q, *J* = 7.4 Hz, 2H, CH_2), 6.46 (d, *J* = 8.8 Hz, 2H, arom), 6.67 (d, *J* = 8.4 Hz, 2H, arom), 6.78 (d, *J* = 8.8 Hz, 2H, arom), 7.05 (d, *J* = 8.4 Hz, 2H, arom), 7.29 (dd, *J* = 4.8 and 7.6 Hz, 1H, arom), 7.67 (dd, *J* = 2.0 and 7.6 Hz, 1H, arom), 8.16 (d, *J* = 1.6 Hz, 1H, arom), 8.22 (dd, *J* = 1.6 and 4.8 Hz, 1H, arom). ^{13}C NMR (methanol-*d*$_4$): δ 13.8, 29.2, 115.5 (2C), 115.9 (2C), 124.7, 131.5 (2C), 133.2 (2C), 135.3, 135.6, 137.4, 139.1, 140.9, 142.9, 146.9, 151.5, 156.9, 157.7. HRMS $C_{21}H_{19}NO_2$ [M+H] calcd: 318.14886, found: 318.14897.

4.1.2.2. 4,4'-(2-(pyridine-3-yl)prop-1-ene-1,1-diyl)diphenol (1b). Bis(4-hydroxyphenyl)methanone (0.50 g, 2.30 mmol) and 1-(pyridin-3-yl)ethan-1-one (**7b**) (0.78 mL, 7.00 mmol) in dry THF (19 mL) were reacted according to **Method A**. The crude was purified by flash column chromatography (petroleum ether/ethyl acetate 3:2, then 1:1, then 2:3) and crystallized from ethyl acetate to give **1b** (0.17 g, yield 24 %), mp > 230 °C. ^{1}H NMR (methanol-*d*$_4$): δ 2.18 (s, 3H, CH_3), 6.50 (d, *J* = 8.4 Hz, 2H, arom), 6.71 (d, *J* = 8.4 Hz, 2H, arom), 6.80 (d, *J* = 8.8 Hz, 2H, arom), 7.08 (d, *J* = 8.0 Hz, 2H, arom), 7.29 (dd, *J* = 5.0 and 7.8 Hz, 1H, arom), 7.71 (d, *J* = 8.0 Hz, 1H, arom), 8.19-8.23 (m, 2H, arom). ^{13}C NMR (methanol-*d*$_4$): δ 23.8, 116.4 (2C), 116.7 (2C), 125.5, 131.5, 132.9 (2C), 134.2 (2C), 136.2, 136.4, 139.6, 143.5, 144.0, 147.6, 151.9, 157.9, 158.4. HRMS $C_{20}H_{17}NO_2$ [M+H] calcd: 304.13321, found: 304.13319.

4.1.2.3. 4,4'-(2-(1H-imidazol-4-yl)but-1-ene-1,1-diyl)diphenol (2a). Bis(4-hydroxyphenyl)methanone (0.50 g, 2.30 mmol) and **10a** (0.29 g, 2.30 mmol) in dry THF (12 mL) were reacted according to **Method B**. The crude was purified by flash column chromatography (petroleum ether/ethyl acetate 1:1, then 3:7, then 2:8) to give **2a** (0.06 g, yield 9 %), mp 147-150 °C. ^{1}H NMR (methanol-*d*$_4$): δ 0.99 (t, *J* = 7.4 Hz, 3H, CH_3), 2.47 (q, *J* = 7.4 Hz, 2H, CH_2), 6.42 (s, 1H, arom), 6.57 (d, *J* = 8.8 Hz, 2H, arom), 6.74 (d, *J* = 8.4 Hz, 2H, arom), 6.80 (d, *J* = 8.4 Hz, 2H, arom), 6.99 (d, *J* = 8.8 Hz, 2H, arom), 7.48 (s, 1H, arom). ^{13}C NMR (methanol-*d*$_4$): δ 14.4, 28.0, 115.7 (2C), 115.9 (2C), 123.6, 131.3 (3C), 132.2 (2C), 135.3, 136.0, 136.4 (2C), 141.1, 157.1, 157.4. HRMS $C_{19}H_{18}N_2O_2$ [M+H] calcd: 307.14410, found: 307.14422.

4.1.2.4. 4,4'-(2-(1H-imidazol-4-yl)prop-1-ene-1,1-diyl)diphenol (2b). Bis(4-hydroxyphenyl)methanone (0.34 g, 1.60 mmol) and **10b** (0.18 g, 1.60 mmol) in dry THF (8 mL) were reacted according to **Method B**. The crude was purified by flash column chromatography (petroleum ether/ethyl acetate 2:3, then 0.5:9.5) to give **2b** (0.07 g, yield 15%) mp 161-162 °C. ^{1}H NMR (methanol-*d*$_4$): δ 2.10 (s, 3H, CH_3), 6.37 (s, 1H, arom), 6.63 (d, *J* = 8.0 Hz, 2H, arom), 6.74 (d, *J* = 8.8 Hz, 2H, arom), 6.84 (d, *J* = 8.8 Hz, 2H, arom), 6.99 (d, *J* = 8.4 Hz, 2H, arom), 7.45 (s, 1H, arom). ^{13}C NMR (methanol-*d*$_4$): δ 21.0, 115.8 (2C), 115.9 (2C), 125.0, 131.9 (3C), 132.2 (2C), 135.2, 135.9, 136.5 (2C), 140.8, 157.3, 157.3 HRMS $C_{18}H_{16}N_2O_2$ [M+H] calcd: 293.12845, found: 293.12837.

4.1.2.5. 4,4'-(2-(pyridine-3-ylmethyl)but-1-ene-1,1-diyl)diphenol (3a). Bis(4-hydroxyphenyl)methanone (0.20 g, 0.90 mmol) and **8a** (0.14 g, 0.90 mmol) in dry THF (4 mL) were reacted according to **Method B**. The crude was purified by flash column chromatography (ethyl acetate) to give **3a** (0.03 g, yield 10 %), mp 202-204 °C. ^{1}H NMR (methanol-*d*$_4$): δ 0.97 (t, *J* = 7.2 Hz, 3H, CH_3), 2.05 (q, *J* = 7.2 Hz, 2H, CH_2), 3.57 (s, 2H, CH_2Py), 6.69-6.72 (m, 4H, arom), 6.97-6.99 (m, 4H, arom), 7.35 (dd, *J* = 4.7 and 7.8 Hz, 1H, arom), 7.66 (d, *J* = 7.6 Hz, 1H, arom), 8.32-8.34 (m, 2H, arom). ^{13}C NMR (methanol-*d*$_4$): δ 13.5, 26.0, 35.5, 115.8 (2C), 115.9 (2C), 125.1, 131.2 (2C), 131.3 (2C), 135.8, 135.9, 137.4, 138.3, 138.7, 141.9, 147.5, 150.1, 157.0, 157.1. HRMS $C_{22}H_{21}NO_2$ [M+H] calcd: 332.16451, found: 332.16485.

4.1.2.6. 4,4'-(2-methyl-3-(pyridin-3-yl)prop-1-ene-1,1-diyl)diphenol (3b). Bis(4-hydroxyphenyl)methanone (0.32 g, 1.50 mmol) and 1-(pyridin-3-yl)propan-2-one (**8b**) (0.20 g, 1.50 mmol) in dry THF (8 mL) were reacted according to **Method B**. The crude was purified by flash column chromatography (petroleum ether/ethyl acetate 1:1) to give **3b** (0.13 g, yield 28 %), mp 205-207 °C. ^{1}H NMR (acetone-*d*$_6$): δ 1.67 (s, 3H, CH_3), 3.52 (s, 2H, CH_2Py), 6.77-6.80 (m, 4H, arom), 7.02 (d, *J* = 8.8

Hz, 2H, arom), 7.06 (d, *J* = 8.4 Hz, 2H, arom), 7.28 (dd, J = 4.8 and 7.7 Hz, 1H, arom), 7.58 (d, *J* = 8.0 Hz, 1H, arom), 8.23 (d, *J* = 8.8 Hz, 1H, arom), 8.39-8.41 (m, 1H, arom). ^{13}C NMR (acetone-*d*$_6$): δ 19.7, 39.0, 115.4 (2C), 115.6 (2C), 124.1, 130.9, 131.1 (2C), 131.3 (2C), 135.1, 135.2, 136.5, 136.9, 140.5, 147.9, 150.6, 156.6, 156.7. HRMS $C_{21}H_{19}NO_2$ [M+H] calcd: 318.14886, found: 318.14866.

4.1.2.7. 4,4'-(2-ethyl-4-(pyridin-3-yl)but-1-ene-1,1-diyl)diphenol (5a). Bis(4-hydroxyphenyl)methanone (0.07 g, 0.30 mmol) and **9a** (0.05 g, 0.30 mmol) in dry THF (1.50 mL) were reacted according to **Method B**. The crude was purified by flash column chromatography (dichloromethane/acetone 9:1) to give **5a** (0.02 g, yield 19 %), mp 210-212 °C. ^{1}H NMR (methanol-*d*$_4$): δ 1.02 (t, *J* = 7.4 Hz, 3H, CH_3), 2.21 (q, *J* = 7.6 Hz, 2H, CH_2), 2.46 (t, *J* = 7.6 Hz, 2H, CH_2), 2.73 (t, *J* = 7.8 Hz, 2H, CH_2), 6.64-6.69 (m, 4H, arom), 6.72-6.75 (m, 2H, arom), 6.84-6.86 (m, 2H, arom), 7.29 (dd, *J* = 4.9 and 7.8 Hz, 1H, arom), 7.46-7.48 (m, 1H, arom), 8.21 (d, *J* = 1.2 Hz, 1H, arom), 8.32 (dd, *J* = 5.2 and 1.6 Hz, 1H, arom). ^{13}C NMR (methanol-*d*$_4$): δ 13.6, 26.0, 32.6, 34.0, 115.7 (2C), 115.8 (2C), 125.0, 131.1 (2C), 131.2 (2C), 136.6, 136.2, 138.4, 138.6, 139.8, 140.7, 147.3, 150.0, 156.8, 156.8. HRMS $C_{23}H_{23}NO_2$ [M+H] calcd: 346.18016, found: 346.17999.

4.1.2.8. 4,4'-(2-methyl-4-(pyridin-3-yl)but-1-ene-1,1-diyl)diphenol (5b). Bis(4-hydroxyphenyl)methanone (0.26 g, 1.20 mmol) and **9b** (0.18 g, 1.20 mmol) in dry THF (6 mL) were reacted according to **Method B**. The crude was purified by flash column chromatography (petroleum ether/ethyl acetate 2:3) to give **5b** (0.18 g, yield 45 %), mp 206-207 °C. ^{1}H NMR (methanol-*d*$_4$): δ 1.81 (s, 3H, CH_3), 2.45 (t, *J* = 7.6 Hz, 2H, CH_2), 2.79 (t, *J* = 7.4 Hz, 2H, CH_2), 6.63-6.70 (m, 6H, arom), 6.81-6.84 (m, 2H, arom), 7.29 (dd, *J* = 4.9 and 7.8 Hz, 1H, arom), 7.50 (d, *J* = 7.6 Hz, 1H, arom), 8.24 (d, *J* = 1.6 Hz, 1H, arom), 8.33 (dd, *J* = 4.8 and 1.6 Hz, 1H, arom). ^{13}C NMR (methanol-*d*$_4$): δ 19.9, 32.4, 37.8, 115.6 (2C), 115.7 (2C), 125.0, 131.4 (2C), 131.5 (2C), 132.3, 136.0, 136.1, 138.4, 139.6, 140.6, 147.3, 150.0, 156.7, 156.8. HRMS $C_{22}H_{21}NO_2$ [M+H] calcd: 332.16451, found: 332.16434.

4.1.2.9. 4,4'-(2-ethyl-4-(1H-imidazol-4-yl)but-1-ene-1,1-diyl)diphenol (6a). Bis(4-hydroxyphenyl)methanone (0.11 g, 0.50 mmol) and **11a** (0.08 g, 0.50 mmol) in dry THF (2.50 mL) were reacted according to **Method B**. The crude was purified by flash column chromatography (petroleum ether/ethyl acetate 0.5:9.5; then ethyl acetate; then ethyl acetate/methanol 8:2) to give **6a** (0.02 g, yield 11 %), mp 139-141 °C. ^{1}H NMR (methanol-*d*$_4$): δ 1.01 (t, *J* = 7.4 Hz, 3H, CH_3), 2.18 (q, *J* = 7.6 Hz, 2H, CH_2), 2.45 (t, *J* = 7.8 Hz, 2H, CH_2), 2.68 (t, *J* = 7.8 Hz, 2H, CH_2), 6.64-6.70 (m, 5H, arom), 6.82 (d, *J* = 8.8 Hz, 2H, arom), 6.89 (d, *J* = 8.4 Hz, 2H, arom), 7.51 (s, 1H, arom). ^{13}C NMR (methanol-*d*$_4$): δ 13.9, 26.0, 26.2, 32.4, 115.9 (2C), 116.0 (3C), 131.5 (2C), 131.5 (2C), 133.8, 136.0, 136.5, 136.6, 139.4, 140.4, 156.9, 156.9. HRMS $C_{21}H_{22}N_2O_2$ [M+H] calcd: 335.17540, found: 335.17552.

4.1.2.10. 4,4'-(4-(1H-imidazol-4-yl)-2-methylbut-1-ene-1,1-diyl)diphenol (6b). Bis(4-hydroxyphenyl)methanone (0.13 g, 0.60 mmol) and **11b** (0.08 g, 0.60 mmol) in dry THF (3 mL) were reacted according to **Method B**. The crude was purified by flash column chromatography (ethyl acetate; then ethyl acetate/methanol 8:2) to give **6b** (0.03 g, yield 16 %), mp 95-99 °C. ^{1}H NMR (methanol-*d*$_4$): 1.78 (s, 3H, CH_3), 2.44 (t, *J* = 7.6 Hz, 2H, CH_2), 2.73 (t, *J* = 7.6 Hz, 2H, CH_2), 6.65-6.68 (m, 5H, arom), 6.78 (d, *J* = 8.8 Hz, 2H, arom), 6.87 (d, *J* = 8.8 Hz, 2H, arom), 7.54 (s, 1H, arom). ^{13}C NMR (methanol-

d4): δ 19.8, 26.1, 36.4, 115.5 (2C), 115.7 (2C), 118.7, 131.5 (2C), 131.7 (2C), 133.1, 135.2, 136.2, 136.4, 137.6, 139.9, 156.7, 156.7. HRMS $C_{20}H_{20}N_2O_2$ [M+H] calcd: 321.15975, found: 321.15967.

4.1.2.11. 4,4'-(2-methylbut-1-ene-1,1-diyl)diphenol (12a). Bis(4-hydroxyphenyl)methanone (0.60 g, 2.80 mmol) and methylethylketone (0.25 mL, 0.20 g, 2.80 mmol) in dry THF (13 mL) were reacted according to **Method B**. The crude was purified by flash column chromatography (petroleum ether/ethyl acetate 3,5:1,5) to give **12a** (0.53 g, yield 73 %) mp 175-176 °C (lit. [40] mp 179-180 °C). ^{1}H NMR: δ 1.03 (t, *J* = 7.4 Hz, 3H, CH_3), 1.76 (s, 3H, CH_3), 2.11 (q, *J* = 7.4 Hz, 2H, CH_2), 4.68 (br, 2H, 2OH), 6.72-6.74 (m, 4H, arom), 6.97-7.00 (m, 4H, arom).

4.1.2.12. 4,4'-(2-methylprop-1-ene-1,1-diyl)diphenol (12b). Bis(4-hydroxyphenyl)methanone (0.60 g, 2.80 mmol) and acetone (0.20 mL, 0.16 g, 2.80 mmol) in dry THF (13 mL) were reacted according to **Method B**. The crude was purified by flash column chromatography (petroleum ether/ethyl acetate 4:1) to give **12b** (0.56 g, yield 83 %) mp 180-182 °C (lit. [40] mp 188-189 °C). ^{1}H NMR: δ 1.79 (s, 6H, $2CH_3$), 4.60 (br, 2H, 2OH), 6.71-6.75 (m, 4H, arom), 6.97-7.00 (m, 4H, arom).

4.1.3. General procedure for the synthesis of compounds 13a,b.

A suspension of **12a** or **12b** (1 eq) and NaH (60 %, 4.1 eq) in dry THF (15-20 mL) was stirred at room temperature for 30 min under an inert N_2 atmosphere. Then, chloromethylmethylether (4 eq) was added and the resulting mixture was stirred at room temperature for 3 hours. The reaction was quenched with aq $NaHCO_3$, the organic solvent was removed under reduced pressure and the aqueous layer was extracted with ethyl acetate. The organic phase was dried and concentrated in vacuum and the crude compound was then purified by flash column chromatography.

4.1.3.1. 4,4'-(2-methylbut-1-ene-1,1-diyl)bis((methoxymethoxy)benzene) (13a). Starting from **12a** (0.53 g, 2.10 mmol), a crude compound was obtained that was purified by flash column chromatography (petroleum ether/ethyl acetate 9.5:0.5) to give **13a** (0.44 g, yield 62 %) as orange oil. ^{1}H NMR: δ 1.03 (t, *J* = 7.4 Hz, 3H, CH_3), 1.76 (s, 3H, CH_3), 2.11 (q, *J* = 7.4 Hz, 2H, CH_2), 3.47 (s, 6H, 2 OCH_3), 5.14 (s, 4H, 2 OCH_2), 6.91-6.95 (m, 4H, arom), 7.01-7.04 (m, 4H, arom).

4.1.3.2. 4,4'-(2-methylprop-1-ene-1,1-diyl)bis((methoxymethoxy)benzene) (13b). Starting from **12b** (0.41 g, 1.70 mmol), a crude compound was obtained that was purified by flash column chromatography (petroleum ether/ethyl acetate 8:2) to give **13b** (0.35 g, yield 62 %) as an oil. ^{1}H NMR: δ 1.79 (s, 6H, 2 CH_3), 3.48 (s, 6H, 2 OCH_3), 5.16 (s, 4H, 2 OCH_2), 6.92-6.95 (m, 4H, arom), 7.02-7.04 (m, 4H, arom).

4.1.4. General procedure for the synthesis of compound 14a,b.

A mixture of **13a** or **13b** (1 eq), N-bromosuccunimide (NBS, 1 eq) and a catalytic amount of benzoyl peroxide (BPO) in CCl_4 (15 mL) was refluxed for 4h. The mixture was hot filtered and evaporated to dryness. The resulting residue, without further purification, was dissolved in acetonitrile and imidazole (3 eq) was added. The reaction mixture was refluxed for 6 h under N_2 atmosphere, the solvent was

evaporated, and the crude compound was purified by flash column chromatography with a suitable eluent.

4.1.4.1. 1-(2-(bis(4-(methoxymethoxy)phenyl)methylene)butyl)-1H-imidazole (14a). Starting from **13a** (0.44 g, 1.30 mmol), a crude compound was obtained that was purified by flash column chromatography (toluene/ethyl acetate 7:3, 1:1, ethyl acetate) to give **14a** (0.10 g, yield 19 % two steps) as brown oil. ^{1}H NMR: δ 0.95 (t, *J* = 7.6 Hz, 3H, CH_3), 2.03 (q, *J* = 7.4 Hz, 2H, CH_2), 3.46 (s, 6H, 2 OCH_3), 4.63 (s, 2H, CH_2-imi), 5.14 (s, 4H, 2 OCH_2), 6.88 (s, 1H, arom), 6.95-6.99 (m, 4H, arom), 7.04-7.07 (m, 5H, arom), 7.45 (s, 1H, arom).

4.1.4.2. 1-(3,3-bis(4-(methoxymethoxy)phenyl)-2-methylallyl)-1H-imidazole (14b). Starting from **13b** (0.35 g, 1.10 mmol), a crude compound was obtained that was purified by flash column chromatography (toluene/ethyl acetate 9:1, 7:3, 1:1, ethyl acetate) to give **14b** (0.08 g, yield 19 % two steps) mp 231-232 °C. ^{1}H NMR: δ 1.71 (s, 3H, 2 CH_3), 3.28 (s, 6H, 2 OCH_3), 4.60 (s, 2H, CH_2-imi), 5.24 (s, 4H, 2 OCH_3), 6.89 (s, 1H, arom), 6.95-6.97 (m, 4H, arom), 7.03-7.05 (m, 5H, arom), 7.47 (s, 1H, arom).

4.1.5. General procedure for the synthesis of compound 4a,b.

To a solution of **14a** or **14b** in methanol (5 mL), 37 % HCl (0.05 mL) was added. The reaction mixture was stirred at room temperature for 12 h and then the solvent was evaporated to dryness. The residue was dissolved in H_2O and neutralized with saturated solution of $NaHCO_3$. The formed precipitate was collected by *vacuum* filtration to afford compound **4a** or **4b**.

4.1.5.1. 4,4'-(2-((1H-imidazol-1-yl)methyl)but-1-ene-1,1-diyl)diphenol (4a). Starting from **14a** (0.10 g, 0.20 mmol), **4a** was obtained (0.06 g, yield 83 %), mp > 250 °C. ^{1}H NMR (acetone-d_6): δ 0.95 (t, *J* = 7.4 Hz, 3H, CH_3), 2.00 (q, *J* = 7.4 Hz, 2H, CH_2), 4.76 (s, 2H, CH_2-imi), 6.79-6.84 (m, 4H, arom), 6.98 (s, 1H, arom), 7.03-7.09 (m, 5H, arom), 7.65 (s, 1H, arom). ^{13}C NMR (acetone-d_6): δ 13.4, 24.0, 47.9, 115.8 (2C), 115.9 (2C),129.2, 130.8 (2C), 131.0 (2C), 131.4, 132.5, 134.2, 134.4, 134.5, 143.6, 157.3, 157.4. HRMS $C_{20}H_{20}N_2O_2$ [M+H] calcd: 321.15975, found: 321.15993.

4.1.5.2. 4,4'-(3-(1H-imidazol-1-yl)-2-methylprop-1-ene-1,1-diyl)diphenol (4b). Starting from **14b**, (0.08 g, 0.20 mmol), **4b** was obtained (0.03 g, yield 30%), mp > 250 °C. ^{1}H NMR (acetone-d_6): δ 1.64 (s, 3H, CH_3), 4.69 (s, 2H, CH_2-imi), 6.79 (d, *J* = 8.6 Hz, 2H, arom), 6.83 (d, *J* = 8.5 Hz, 2H, arom), 6.93 (s, 1H, arom), 6.99-7.02 (m, 3H, arom), 7.06 (d, *J* = 8.5 Hz, 2H, arom), 7.51 (s, 1H, arom), 8.39 (br, 1H, OH), 8.45 (br, 1H, OH). ^{13}C NMR (acetone-d_6): δ 17.9, 51.2, 115.6 (2C), 116.0 (2C), 119.6, 128.6, 129.8, 131.4 (2C), 131.4 (2C), 134.2, 134.5, 138.2, 142.8, 157.3, 157.4. HRMS $C_{19}H_{18}N_2O_2$ [M+H] calcd: 307.14410, found: 307.14464.

4.1.6. 1-(pyridine-3-yl)butan-2-one (8a). A solution of 2-(pyridine-3-yl)acetic acid (0.58 g, 4.20 mmol), pyridine (2 mL) and propionic anhydride (2 mL) was refluxed under N_2 for 6 h. Solvents were evaporated and the residue was dissolved in dichlorometane and washed with 2M NaOH solution. The organic layer

was dried and concentrated *in vacuum* and the crude compound was purified by flash chromatography (ethyl acetate) to give **8a** (0.14 g, yield 22 %) like a yellow oil. ^{1}H NMR: δ 1.07 (t, *J* = 6.8 Hz, 3H, CH_3), 2.53 (q, *J* = 6.8 Hz, 2H, CH_2), 3.71 (s, 2H, CH_2Py), 7.22-7.30 (m, 1H, arom), 7.55 (dd, *J* = 1.7 and 7.9 Hz, 1H, arom), 8.45 (d, *J* = 1.8 Hz, 1H, arom), 8.52 (d, *J* = 7.6 Hz, 1H, arom).

4.1.7. General procedure for the synthesis of compounds 15-16a,b.

A solution of the selected aldehyde (1 eq), piperidine (1.8 eq) and acetic acid (1.6 eq) in acetone or methylethylketone was stirred at room temperature until TLC indicated complete conversion of the starting material. The solvent was evaporated to dryness and the obtained crude compound was purified by flash column chromatography with a suitable eluent.

4.1.7.1. (E)-1-(pyridin-3-yl)pent-1-en-3-one (15a). Starting from 3-pyridinecarboxyaldehyde (1,00 g, 0.88 mL, 9.30 mmol) in methylethylketone (20 mL), a crude was obtained that was purified by flash column chromatography (toluene/acetone 6:4) to give **15a** (0.48 g, yield 32 %) as brown oil. ^{1}H NMR: δ 1.18 (t, *J* = 7.2 Hz, 3H, CH_3), 2.72 (q, *J* = 7.2 Hz, 2H, CH_2), 6.81 (d, *J* = 16.4 Hz, 1H, CH=C), 7.34-7.37 (m, 1H, arom), 7.55 (d, *J* = 16.4 Hz, 1H, CH=C), 7.88 (d, *J* = 8.0 Hz, 1H, arom), 8.62-8.64 (m, 1H, arom), 8.78 (s, 1H, arom).

4.1.7.2. (E)-4-(pyridin-3-yl)but-3-en-2-one (15b). Starting from 3-pyridinecarboxyaldehyde (0.50 g, 0.44 mL, 4.70 mmol) in acetone (8 mL), a crude was obtained that was purified by flash column chromatography (petroleum ether/ethyl acetate 1:9, 0.5:9.5, ethyl acetate) to give **15b** (0.38 g, yield 55 %) as brown oil. ^{1}H NMR: δ 2.38 (s, 3H, CH_3), 6.76 (d, *J* = 16.4 Hz, 1H, CH=C), 7.30-7.46 (m, 1H, arom), 7.48 (d, *J* = 16.4 Hz, 1H, CH=C), 7.84 (d, *J* = 8.0 Hz, 1H, arom), 8.59 (d, *J* = 4.4 Hz, 1H, arom), 8.74 (s, 1H, arom).

4.1.7.3. (E)-1-(1H-imidazol-4-yl)pent-1-en-3-one (16a). Starting from 1H-imidazole-4-carboxyaldehyde (0.50 g, 5.20 mmol) in methylethylketone (10 mL), a crude compound was obtained that was purified by flash column chromatography (dichlorometane/methanol 8:2) to give **16a** (0.70 g, yield 89 %) as brown oil. ^{1}H NMR (methanol-*d*$_4$): δ 1.14 (t, *J* = 7.2 Hz, 3H, CH_3), 2.75 (q, *J* = 7.2 Hz, 2H, CH_2), 6.88 (d, *J* = 16.8 Hz, 1H, CH=C), 7.53 (d, *J* = 16.0 Hz, 1H, CH=C), 7.92 (s, 1H, arom), 9.04 (s, 1H, arom).

4.1.7.4. (E)-4-(1H-imidazol-4-yl)but-3-en-2-one (16b). Starting from 1H-imidazole-4-carboxyaldehyde (0.50 g, 5.20 mmol) in acetone (10 mL), a crude compound was obtained that was purified by flash column chromatography (acetone + 0.5 % NH_3) to give **16b** (0.24 g, yield 34 %) as brown oil. ^{1}H NMR: δ 2.31 (s, 3H, CH_3), 6.75 (d, *J* = 16.0 Hz, 1H, CH=C), 7.34 (s, 1H, arom), 7.47 (d, *J* = 16.0 Hz, 1H, CH=C), 7.72 (s, 1H, arom).

4.1.8. General procedure for the synthesis of compounds 9a,b and 11a,b.

A mixture of **15a,b** or **16a,b** (1 eq) and Zn (5 eq) in acetic acid (10-15 mL) was heated to reflux for 3 h. The reaction mixture was poured in water, basified with 2M NaOH solution and extracted with dichlorometane. The organic phase was washed with $NaHCO_3$ saturated solution, dried over anhydrous Na_2SO_4 and concentrated in vacuum. The crude compound, when necessary, was purified by flash column chromatography with a suitable eluent.

4.1.8.1. 1-(pyridin-3-yl)pentan-3-one (9a). Starting from **15a** (0.48 g, 2.80 mmol), a crude compound was obtained and was purified by column chromatography (toluene/acetone 7:3) to give **9a** (0.29 g, yield 62 %) as brown oil. ^{1}H NMR: δ 1.04 (t, *J* = 7.4 Hz, 3H, CH_3), 2.41 (q, *J* = 7.4 Hz, 2H, CH_2), 2.74 (t, *J* = 7.4 Hz, 2H, CH_2), 2.90 (t, *J* = 7.4 Hz, 2H, CH_2), 7.18-7.22 (m, 1H, arom), 7.51 (d, *J* = 8.0 Hz, 1H, arom), 8.44-8.46 (m, 2H, arom).

4.1.8.2. 4-(pyridin-3-yl)butan-2-one (9b). Starting from **15b** (0.41 g, 2.80 mmol), a crude compound was obtained that was used without further purification (0.18 g, yield 43 %) as brown oil. ^{1}H NMR: δ 2.15 (s, 3H, CH_3), 2.79 (t, *J* = 7.2 Hz, 2H, CH_2), 2.92 (t, *J* = 7.4 Hz, 2H, CH_2), 7.27-7.29 (m, 1H, arom), 7.61 (d, *J* = 7.6 Hz, 1H, arom), 8.46-8.48 (m, 2H, arom).

4.1.8.3. 1-(1H-imidazol-4-yl)pentan-3-one (11a). Starting from **16a** (0.35 g, 2.30 mmol), a crude compound was obtained and was purified by column chromatography (dichlorometane/methanol 9:1) to give **11a** (0.15 g, 43 %) as brown oil. ^{1}H NMR: 1.06 (t, *J* = 7.4 Hz, 3H, CH_3), 2.45 (q, *J* = 7.4 Hz, 2H, CH_2), 2.82 (t, *J* = 6.0 Hz, 2H, CH_2), 2.89 (t, *J* = 6.0 Hz, 2H, CH_2), 4.17 (br, 1H, NH), 6.82 (s, 1H, arom), 7.66 (s, 1H, arom).

4.1.8.4. 4-(1H-imidazol-4-yl)butan-2-one (11b). Starting from **16b** (0.18 g, 1.30 mmol), a crude compound was obtained that was used without further purification (0.12 g, 66 %) as brown oil. ^{1}H NMR: δ 2.16 (s, 3H, CH_3), 2.78-2.86 (m, 4H, 2 CH_2), 6.80 (s, 1H, arom), 7.65 (s, 1H, arom).

4.1.9. 1-(1H-imidazol-4-yl)ethan-1-one (10b). 4(5)-cyanoimidazole [41] (0.48 g, 5.20 mmol) in THF (5 mL) was added to a 3M solution of methylmagnesium bromide (8.6 mL, 26 mmol) and the mixture was stirred at rt for 3h. Then, H_2O and 10 % H_2SO_4 solution were added dropwise and the mixture was stirred for 30 min and then brought to pH 8 with 30 % NaOH solution. After the organic layer was separated, the aqueous layer was extracted with ethyl acetate. The organic layers were combined, washed with $NaHCO_3$ saturated solution and brine, and concentrated under reduced pressure. The crystals formed were collected by filtration to give **10b** (0.30 g, yield 53 %) mp 179-180 °C (lit. [42] mp 172 °C). ^{1}H NMR: δ 2.52 (s, 3H, CH_3), 7.76 (s, 1H, arom), 7.80 (s, 1H, arom).

4.2. Biological Assays

4.2.1. Aromatase inhibition assays

Inhibition of HA was quantified by the Aromatase Inhibitor Screening Kit (BioVision Inc., San Francisco, USA), monitoring the conversion of a fluorogenic substrate into a highly fluorescent metabolite as catalyzed by the AR enzyme. After the reconstitution of the reagents, a standard curve was

generated by diluting the fluorescent standard. Test compounds were dissolved in DMSO at a final concentration of ≤ 0.25 % (v/v), after having verified that such concentration of solvent does not significantly affect the activity of the enzyme. Each mother solution was diluted in the assay buffer to generate a range of concentrations instrumental to build a multi-point dose-response curve. The reaction was prepared by adding Aromatase mix (containing Recombinant Human Aromatase (2X), the aromatase assay buffer as well as NADPH-generating system) to test compounds, inhibitor control, background control and positive control (1 µM LTZ). The reaction mixture was preincubated at 37 °C for 10 min in order to allow the tested inhibitors to interact with the enzyme. Subsequently, the reaction initiated after the addition of 30 µL of aromatase substrate/NADP+ mixture (containing buffer, aromatase substrate and β-$NADP^+$ 100X stock). The assays were done in 96-well microtiter plates (Corning Incorporated, Corning, ME, USA) in a final reaction volume of 100 µL/well. The fluorescence of the sample was measured using a TECAN Ultra microplate reader (Tecan Trading AG, Switzerland) at dual wavelengths of 488/527 nm for 60 min. Results were expressed as relative fluorescence units (RFUs). Experiments were carried out in triplicate and the average values were used to construct the dose-response curves. The percentage of inhibition was calculated as the ratio between the RFUs of control and test compound, according to the manufacturer's instructions. Tests were done at different concentrations (10, 1, 0.1, 0.01 0.001 and 0.0001 µM). For each compound, the concentration able to inhibit enzymatic activity by 50 % (IC_{50}) was calculated by nonlinear regression of the experimental data to a tetraparametric logistic curve (SigmaPlot 13.0 - Systat Software Inc.). In order to test the sensitivity of the kit and assess the quality of the measurements the IC_{50} of letrozole and END were also tested with the same procedure.

4.2.2. Estrogen receptor binding assays

The PolarScreen ERα Competitor Assay Kit Green (Cat.No.15883; Invitrogen) was used to determine the relative affinity of tested compounds, of the reference SERM END and of letrozole (as a negative control) towards ERα, according to the manufacturer's protocol. Briefly, serial dilutions of each test compound (10-0.001 µM) were prepared at 100X in 100 % DMSO in a DMSO tolerant plate. The compounds were further diluted 50-fold in screening buffer to get a 2X final concentration and 2 % DMSO. Ten µL of the 2X compound concentration was added to a 10 µL mixture containing 2X full length ERα and Fluormone™ ES2 Green (75 nM ERα; 4.5 nM Fluormone™ ES2 Green) in a black low volume 384-well assay plate (Corning NY, US) to obtain 20 µL final volume. The negative control contained 10 µL of screening buffer and 10 µL of ERα/Fluormone™ ES2 Green Complex. This control was used to determine the polarization value when no competitor was present (theoretical maximum polarization). Ten µL of ERα/Fluormone™ ES2 Green Complex and 10 µL of 20 µM β-estradiol (endogenous ligand) (final concentration in well of 10 µM) were used as a positive control (minimum polarization value). The assay plate was then incubated in the dark at room temperature for 2h. Polarization values were measured on a Tecan Spark Plate Reader with 485 nm excitation and 530 nm emission interference filters with bandwidths of 25/20 nm. All measurements were done in triplicate. The polarization values were converted to percent inhibition using the equation:

$I\% = (P_0–P)/(P_0–P_{100}) \times 100$,

where P_0 is the polarization value at 0 % inhibition, P_{100} is the polarization value at 100 % inhibition, and P is the observed FP at each concentration point. We used free β-estradiol (100 % inhibition) as a positive

control and ERα/Fluormone™ ES2 Green Complex (0 % inhibition) as a negative control. We transformed polarization values into percent inhibition to normalize the differences at 0 % inhibition for each run.

We then analyzed the percent inhibition versus competitor concentration curves by nonlinear least-squares curve fitting and determined the concentration of competitor needed to displace half of the bound ligand (IC_{50}). IC_{50} values were calculated using GraphPad Prism software.

4.2.3. Cell lines and culture conditions

MCF-7 and MCF10A cell lines were obtained from American Type Culture Collection (ATCC). MCF-7 cells were grown in RPMI + 10 % FBS, while MCFA10 in in MEBM medium (Lonza) supplemented with 10ng/mL EGF, 10ng/mL FGF, 600 U/L eparin and B-27 Supplement (Thermo Fisher Scientific). Cells were tested for the absence of *Mycoplasma* fortnightly and maintained in logarithmic growth phase as a monolayer in a humidified 5 % CO2 atmosphere at 37°C.

4.2.4. Cell proliferation assays

Cells were seeded in triplicate in 12-well plates (50.000 cells/well, 70.000 cells/well, 90.000 cells/well for MDA-MB-231 cells and MCF-7 cells, and MCF10A, respectively). After 24 h cells were exposed to increasing concentrations of compounds **1a-6b** and of the two reference compounds letrozole and END for 72 h. Culture medium was then removed and adherent cells were harvested using trypsin and counted with a cell counter (Beckman Coulter, S.p.A., Milan, Italy). All experiments were performed in triplicate. The IC_{50} value was defined as the concentration of a drug inhibiting cell proliferation by 50 %.

4.2.5. Progesteron receptor (PGR) mRNA expression analysis

MCF-7 cells were seeded at a density of 10^5 cells/well in a six well plate and preconditioned with minimum essential media (MEM) supplemented with 10% charcoal-stripped FBS 72 h before treatment, to remove the estrogens from the culture medium containing 10% FBS. Cells were treated with 10 nM estradiol (E2) alone, or in combination with i) 1 μM endoxifen, used as positive control, ii) **3a** 10 or 20 μM, iii) **6a** 10 or 20 μM. After 24 h from treatment, cells treated with E2 in combination with the tested compounds or endoxifen were harvested for RNA extraction using PureLink™ RNA Mini Kit (Thermo Fisher Scientific, Invitrogen, Waltham, MA, USA), according to manufacturer's instructions. Briefly, cells were lysed using Lysis Buffer supplemented with 1% β-mercaptoethanol. Lysed samples were added to an equal volume of ethanol and mixed thoroughly. The solution was passed through a filter cartridge containing a silica-based membrane to which RNA binds. The membranes were then washed with Wash Buffer I and two times with Wash Buffer II. Total RNA was finally eluted with RNase-free water and stored at -20°C. RNA was quantified using the Nanoquant plate (Tecan, Männedorf, Switzerland) using the multiplate reader Infinite 200 PRO (Tecan). Complementary DNA (cDNA) was synthetized using the High-Capacity cDNA Reverse Transcription kit (Life Technologies, Carlsbald, CA, USA). Briefly, 200 ng of RNA in a total volume of 10 μL in RNase free water were added to 10 μL of master mix prepared according to manufacturer's instructions with RNase inhibitor and subjected to appropriate thermocycling conditions using MiniAmp thermal cycler (Thermo Fisher Scientific). Finally, relative quantification was performed by real time PCR (BIORAD CFX Connect,) using Universal Master Mix (Themo Fisher Scientific) and Taqman gene expression assay (Thermo Fisher Scientific) for

PGR gene (FAM, Hs01556702_m1) and glyceraldehyde 3-phosphate dehydrogenase gene (GADPH, FAM, Hs99999905_m1), used as endogenous control to normalize each sample. Each measurement was performed in duplicate for a total of 40 amplification cycles. Quantitative values of amplification were obtained from the threshold cycle (Ct), defined as the number of cycles required for the fluorescent signal to exceed the background level. The relative mRNA expression was analyzed using the $2^{-\Delta\Delta Ct}$ method (Livak KJ, Schmittgen TD (2001). Analysis of relative gene expression data using real-time quantitative PCR and the 2(-Delta Delta C(T)) Method. Methods, 25(4): 402–8) and untreated MCF-7 cells were used as calibrator of the experiment. The results were expressed as percentage of antiestrogenic effects compared to E2-stimulated mRNA expression of PGR, considered as 100%.

4.2.6. Protein extraction and western blot analysis

MCF-7 cells were incubated with vehicle (DMSO), test compounds (IC_{50} calculated by ERα binding assay) or fulvestrant (1 µM) for 72h. Then, cells were harvested using a scraper and lysed with RIPA buffer (Thermo Scientific Pierce, #89900). Protein samples were sonicated for 20 s and quantified through the BCA assay method (Thermo Fisher Scientific, Waltham, MA, USA). Total cellular lysates were separated on a 4–12% NuPAGE bis-tris gel (Thermo Fisher Scientific, Waltham, MA, USA) and transferred to nitrocellulose using standard protocols. Filters were blocked in PBS-Tween 20 with 5% skim milk and incubated overnight with primary antibodies specific for ERα (ab16660; Abcam, Cambridge, UK). β-actin (ab8226; Abcam, Cambridge, UK) antibody was used to confirm equal protein loading on the gel. Band density was quantified by scanning films and processing image intensities with the ImageJ 1.47v Software.

4.3. Computational details

4.3.1. Docking calculations

Docking simulations of compounds **1a-6b** on aromatase enzyme were performed with Glide [43] using the single precision (SP) protocol on the AR crystal structure (PDB code 3S79). A van der Waals (vdW) radius scaling factor of 0.80 Å for protein and ligands atoms having a partial charge less than 0.15 was used to mimic protein flexibility. A metal constraint was incorporated in order to mimic a binding pose in which the nitrogen atom was at coordination distance from the heme iron atom, as in previous study [35]. Possible tautomerism of the imidazole ring of **2a-b** and **6a-b** have been explicitly considered.

In order to predict the binding mode of the newly synthesized compound to ERα we used the structure of ERα in complex with END obtained from MD simulations of our previous study [6]. The **1a-6b** compounds were docked in the LBD cavity of ERα with the Glide software using the same protocol detailed above for AR. Validation of the protocol has been performed reproducing the binding poses of endoxifen and exemestane, as extracted from their crystallographic structures bound to ERα [44] and AR [10], respectively (See Table S1).

4.3.2. Classical MD simulations of AR

We performed classical MD simulations on selected models of AR in complex with the docked inhibitors, using a protocol adopted in previous studies [45]. Namely, the protonation states under physiological

conditions were calculated with the webserver H++ [46], while Asp309 was considered its neutral form, as reported in literature [47, 48]. We have used Parm99SB AMBER force field for the protein [49, 50], the Shahrokh *et al.* parameters for the heme moiety and Cys437 [51] and the general Amber FF (GAFF) for the inhibitors [52]. The ESP charges [53] were derived by performing geometry optimization of the inhibitors at Hartree-Fock level of theory with a 6-31G* basis set using the Gaussian 09 software and were subsequently transformed in RESP charges by Antechamber module of Ambertools 18 [54]. Our models were solvated along the x and y direction with the TIP3P waters model [55] leading to a total of 66342 atoms. The systems topology was built with Ambertools 18, and later converted to a GROMACS format with the software acpype.

The GROMACS 2018.2 [56] code was finally used to perform 100 ns MD simulations using an integration time step of 2 fs and all covalent bonds involving hydrogen atoms constrained with the LINCS algorithm. MD simulations were done in the NPT ensemble, at a temperature of 300 K, using a velocity-rescaling thermostat [57]. An initial energy minimization step was done with the steepest descend algorithm. A preliminary equilibration of the model was performed for 20 ns with the protein and ligand atoms harmonically restrained using a force constant of 1000 kJ mol^{-1} nm^{-2}. Next, constraints were released, and the model was thermalized to the target temperature of 300 K within 10 ns. In order to relax the AR structure to the presence of the ligand and monitor the stability of the docking poses each system underwent by 100 ns-long MD simulation, while keeping restrained the distance of the ligand to the Fe of the heme moiety.

4.3.3. QM/MM Molecular Dynamics Simulations of AR

Due to the difficulties in describing coordination bonds with classical FF [58, 59], QM/MM Born Oppenheimer MD simulations were performed using CP2K 6.1 program [60-62]. The QM layer, including the heme group and the inhibitors (90 atoms), was simulated in a cubic box with sides of 24 Å and it was described at Density Functional Theory (DFT) using the BLYP [63, 64] exchanges correlation functional with a dual Gaussian-type/Plane Waves basis set (GPW) [65]. In particular, we employed a double ζ (MOLOPT) basis set, an auxiliary PW basis set with a density cutoff of 400 Ry and Goedecker-Teter-Hutter (GTH) pseudopotentials [66, 67]. This protocol has been used successfully in many QM/MM MD simulations of biomolecules, including aromatase [45, 68, 69]. The dangling bonds between the quantum and classical regions were saturated using capping hydrogens atoms. An integration step of 0.5 fs was used in all the QM/MM MD simulations in the NVT ensemble. All systems were initially optimized and equilibrated at 300 K without constraints for 2 ps, using a Nosé-Hoover thermostat [70], followed by other 8 ps after the stable formation of the coordination bond has occurred. The heme iron atom was simulated with a doublet spin state, consistently with other studies [35]. The MM region was described with the same force field of the classical MD simulations.

4.3.4. Classical MD Simulations of ERα

After docking the inhibitor to the LBD of ERα monomer. The antagonist adducts in its dimeric form was built on the crystal structures of ERα the LDB dimer in the antagonist state by superimposing this monomeric antagonist ERαs structures, on the both monomers of the antagonist ERα crystal structure (PDB id: 1qku), following an established computational protocol [6]. Nonetheless, we verified the

stability of the built dimers for each complex 500 ns of MD simulations. Each model of the drug/ERα was solvated with TIP3P water molecules in the rectangular shaped box with the dimensions of at least 12 Å in each direction from the solute, and charge neutrality was achieved by the addition of Na^+ ions [71], leading to a total of 60000 atoms. In all simulations we used the same protocol detailed above.

4.3.5. Analysis

Cluster analysis and root mean square deviation (RMSD) of the MD trajectories were carried out using g_cluster tool, based on the Daura et. al algorithm [72] and g_rmsd gmx_rmsf modules of the GROMACS 2018.2 package. The *cpptraj* module of Amber program was used for hydrogen bond analysis (cut-off parameters for H-bond was 3.3 Å and 35°), cross-correlation matrices. As in previous studies we have introduced a simplified form of the cross correlation matrix in which the cross correlation coefficients are summed by structural elements [6, 73].

The Amber 18 tool MM_PBSA.py [74] was used to perform Molecular Mechanics Generalized Born Surface Area (MM-GBSA) free energy calculation, taking 500 frames from an equilibrated part of the MD trajectories. An improved generalized born solvation model was employed (igb=8) [75], and a salt concentration of 0.1 M. The conformational entropic contribution of the free energy was not considered, as it was suggested that this term does not improve the quality of the results using the MM-G(P)BSA [76, 77]. Visualization of the MD trajectories and images were done using the VMD program [78] and UCSF Chimera [79].

5. Supplementary Data

Figures S1-S6, Tables S1-S9, ligand parameters, synthetic schemes S1-S3 and representative NMR spectra of studied compounds (**3a**).

Acknowledgments

AM thanks the Italian Association for Cancer Research (AIRC, MFAG Grant No 17134). AS was supported by a FIRC-AIRC 'Mario e Valeria Rindi' fellowship for Italy.

References

1. American Cancer Society. Cancer Facts & Figures 2020. Atlanta, 2020.
2. American Cancer Society. Breast Cancer Facts & Figures 2019-2020. Atlanta, 2019.
3. Feng, Y.; Spezia, M.; Huang, S.; Yuan, C.; Zeng, Z.; Zhang, L.; Ji, X.; Liu, W.; Huang, B.; Luo, W.; Liu, B.; Lei, Y.; Du, S.; Vuppalapati, A.; Luu, H. H.; Haydon, R. C.; He, T. C.; Ren, G., Breast cancer development and progression: Risk factors, cancer stem cells, signaling pathways, genomics, and molecular pathogenesis. *Genes Dis* **2018,** *5* (2), 77-106.
4. Spinello, A.; Ritacco, I.; Magistrato, A., The Catalytic Mechanism of Steroidogenic Cytochromes P450 from All-Atom Simulations: Entwinement with Membrane Environment, Redox Partners, and Post-Transcriptional Regulation. *Catalysts* **2019,** *9* (1).

5. Heldring, N.; Pike, A.; Andersson, S.; Matthews, J.; Cheng, G.; Hartman, J.; Tujague, M.; Ström, A.; Treuter, E.; Warner, M.; Gustafsson, J. A., Estrogen receptors: how do they signal and what are their targets. *Physiol Rev* **2007,** *87* (3), 905-31.
6. Pavlin, M.; Spinello, A.; Pennati, M.; Zaffaroni, N.; Gobbi, S.; Bisi, A.; Colombo, G.; Magistrato, A., A Computational Assay of Estrogen Receptor α Antagonists Reveals the Key Common Structural Traits of Drugs Effectively Fighting Refractory Breast Cancers. *Sci Rep* **2018,** *8* (1), 649.
7. Patel, H. K.; Bihani, T., Selective estrogen receptor modulators (SERMs) and selective estrogen receptor degraders (SERDs) in cancer treatment. *Pharmacol Ther* **2018,** *186*, 1-24.
8. Barros-Oliveira, M. D. C.; Costa-Silva, D. R.; Andrade, D. B.; Borges, U. S.; Tavares, C. B.; Borges, R. S.; Silva, J. M.; Silva, B. B. D., Use of anastrozole in the chemoprevention and treatment of breast cancer: A literature review. *Rev Assoc Med Bras (1992)* **2017,** *63* (4), 371-378.
9. Van Asten, K.; Neven, P.; Lintermans, A.; Wildiers, H.; Paridaens, R., Aromatase inhibitors in the breast cancer clinic: focus on exemestane. *Endocr Relat Cancer* **2014,** *21* (1), R31-49.
10. Ghosh, D.; Lo, J.; Morton, D.; Valette, D.; Xi, J.; Griswold, J.; Hubbell, S.; Egbuta, C.; Jiang, W.; An, J.; Davies, H. M., Novel aromatase inhibitors by structure-guided design. *J Med Chem* **2012,** *55* (19), 8464-76.
11. Egbuta, C.; Lo, J.; Ghosh, D., Mechanism of inhibition of estrogen biosynthesis by azole fungicides. *Endocrinology* **2014,** *155* (12), 4622-8.
12. Spinello, A.; Martini, S.; Berti, F.; Pennati, M.; Pavlin, M.; Sgrignani, J.; Grazioso, G.; Colombo, G.; Zaffaroni, N.; Magistrato, A., Rational design of allosteric modulators of the aromatase enzyme: An unprecedented therapeutic strategy to fight breast cancer. *Eur J Med Chem* **2019,** *168*, 253-262.
13. Hadji, P.; Aapro, M. S.; Body, J. J.; Gnant, M.; Brandi, M. L.; Reginster, J. Y.; Zillikens, M. C.; Glüer, C. C.; de Villiers, T.; Baber, R.; Roodman, G. D.; Cooper, C.; Langdahl, B.; Palacios, S.; Kanis, J.; Al-Daghri, N.; Nogues, X.; Eriksen, E. F.; Kurth, A.; Rizzoli, R.; Coleman, R. E., Management of Aromatase Inhibitor-Associated Bone Loss (AIBL) in postmenopausal women with hormone sensitive breast cancer: Joint position statement of the IOF, CABS, ECTS, IEG, ESCEO IMS, and SIOG. *J Bone Oncol* **2017,** *7*, 1-12.
14. Foglietta, J.; Inno, A.; de Iuliis, F.; Sini, V.; Duranti, S.; Turazza, M.; Tarantini, L.; Gori, S., Cardiotoxicity of Aromatase Inhibitors in Breast Cancer Patients. *Clin Breast Cancer* **2017,** *17* (1), 11-17.
15. Ewer, M. S.; Glück, S., A woman's heart: the impact of adjuvant endocrine therapy on cardiovascular health. *Cancer* **2009,** *115* (9), 1813-26.
16. Lewis-Wambi, J. S.; Jordan, V. C., Treatment of Postmenopausal Breast Cancer with Selective Estrogen Receptor Modulators (SERMs). *Breast Dis* **2005,** *24*, 93-105.
17. Martinkovich, S.; Shah, D.; Planey, S. L.; Arnott, J. A., Selective estrogen receptor modulators: tissue specificity and clinical utility. *Clin Interv Aging* **2014,** *9*, 1437-52.
18. Ring, A.; Dowsett, M., Mechanisms of tamoxifen resistance. *Endocr Relat Cancer* **2004,** *11* (4), 643-58.
19. Shagufta; Ahmad, I., Tamoxifen a pioneering drug: An update on the therapeutic potential of tamoxifen derivatives. *Eur J Med Chem* **2018,** *143*, 515-531.
20. Toy, W.; Weir, H.; Razavi, P.; Lawson, M.; Goeppert, A. U.; Mazzola, A. M.; Smith, A.; Wilson, J.; Morrow, C.; Wong, W. L.; De Stanchina, E.; Carlson, K. E.; Martin, T. S.; Uddin, S.; Li, Z.; Fanning, S.; Katzenellenbogen, J. A.; Greene, G.; Baselga, J.; Chandarlapaty, S., Activating. *Cancer Discov* **2017,** *7* (3), 277-287.
21. Lei, J. T.; Gou, X.; Seker, S.; Ellis, M. J., alterations and metastasis in estrogen receptor positive breast cancer. *J Cancer Metastasis Treat* **2019,** *5*.

22. Pavlin, M.; Gelsomino, L.; Barone, I.; Spinello, A.; Catalano, S.; Andò, S.; Magistrato, A., Structural, Thermodynamic, and Kinetic Traits of Antiestrogen-Compounds Selectively Targeting the Y537S Mutant Estrogen Receptor α Transcriptional Activity in Breast Cancer Cell Lines. *Front Chem* **2019,** *7*, 602.
23. Hamilton, E. P.; Patel, M. R.; Armstrong, A. C.; Baird, R. D.; Jhaveri, K.; Hoch, M.; Klinowska, T.; Lindemann, J. P. O.; Morgan, S. R.; Schiavon, G.; Weir, H. M.; Im, S. A., A First-in-Human Study of the New Oral Selective Estrogen Receptor Degrader AZD9496 for ER. *Clin Cancer Res* **2018,** *24* (15), 3510-3518.
24. Jelovac, D.; Macedo, L.; Goloubeva, O. G.; Handratta, V.; Brodie, A. M., Additive antitumor effect of aromatase inhibitor letrozole and antiestrogen fulvestrant in a postmenopausal breast cancer model. *Cancer Res* **2005,** *65* (12), 5439-44.
25. Baum, M.; Buzdar, A.; Cuzick, J.; Forbes, J.; Houghton, J.; Howell, A.; Sahmoud, T.; ATAC (Arimidex, T. m. A. o. i. C. T. G., Anastrozole alone or in combination with tamoxifen versus tamoxifen alone for adjuvant treatment of postmenopausal women with early-stage breast cancer: results of the ATAC (Arimidex, Tamoxifen Alone or in Combination) trial efficacy and safety update analyses. *Cancer* **2003,** *98* (9), 1802-10.
26. Howell, A.; Cuzick, J.; Baum, M.; Buzdar, A.; Dowsett, M.; Forbes, J. F.; Hoctin-Boes, G.; Houghton, J.; Locker, G. Y.; Tobias, J. S.; Group, A. T., Results of the ATAC (Arimidex, Tamoxifen, Alone or in Combination) trial after completion of 5 years' adjuvant treatment for breast cancer. *Lancet* **2005,** *365* (9453), 60-2.
27. Lu, W. J.; Desta, Z.; Flockhart, D. A., Tamoxifen metabolites as active inhibitors of aromatase in the treatment of breast cancer. *Breast Cancer Res Treat* **2012,** *131* (2), 473-81.
28. Lu, W. J.; Xu, C.; Pei, Z.; Mayhoub, A. S.; Cushman, M.; Flockhart, D. A., The tamoxifen metabolite norendoxifen is a potent and selective inhibitor of aromatase (CYP19) and a potential lead compound for novel therapeutic agents. *Breast Cancer Res Treat* **2012,** *133* (1), 99-109.
29. Lv, W.; Liu, J.; Skaar, T. C.; O'Neill, E.; Yu, G.; Flockhart, D. A.; Cushman, M., Synthesis of Triphenylethylene Bisphenols as Aromatase Inhibitors That Also Modulate Estrogen Receptors. *J Med Chem* **2016,** *59* (1), 157-70.
30. Lubczyk, V.; Bachmann, H.; Gust, R., Investigations on estrogen receptor binding. The estrogenic, antiestrogenic, and cytotoxic properties of C2-alkyl-substituted 1,1-bis(4-hydroxyphenyl)-2-phenylethenes. *J Med Chem* **2002,** *45* (24), 5358-64.
31. Recanatini, M.; Bisi, A.; Cavalli, A.; Belluti, F.; Gobbi, S.; Rampa, A.; Valenti, P.; Palzer, M.; Palusczak, A.; Hartmann, R. W., A new class of nonsteroidal aromatase inhibitors: design and synthesis of chromone and xanthone derivatives and inhibition of the P450 enzymes aromatase and 17 alpha-hydroxylase/C17,20-lyase. *J Med Chem* **2001,** *44* (5), 672-80.
32. Gobbi, S.; Cavalli, A.; Negri, M.; Schewe, K. E.; Belluti, F.; Piazzi, L.; Hartmann, R. W.; Recanatini, M.; Bisi, A., Imidazolylmethylbenzophenones as highly potent aromatase inhibitors. *J Med Chem* **2007,** *50* (15), 3420-2.
33. Gobbi, S.; Zimmer, C.; Belluti, F.; Rampa, A.; Hartmann, R. W.; Recanatini, M.; Bisi, A., Novel highly potent and selective nonsteroidal aromatase inhibitors: synthesis, biological evaluation and structure-activity relationships investigation. *J Med Chem* **2010,** *53* (14), 5347-51.
34. Catanzaro, E.; Seghetti, F.; Calcabrini, C.; Rampa, A.; Gobbi, S.; Sestili, P.; Turrini, E.; Maffei, F.; Hrelia, P.; Bisi, A.; Belluti, F.; Fimognari, C., Identification of a new tamoxifen-xanthene hybrid as pro-apoptotic anticancer agent. *Bioorg Chem* **2019,** *86*, 538-549.
35. Caciolla, J.; Spinello, A.; Martini, S.; Bisi, A.; Zaffaroni, N.; Gobbi, S.; Magistrato, A., Targeting Orthosteric and Allosteric Pockets of Aromatase via Dual-Mode Novel Azole Inhibitors. *ACS Med Chem Lett* **2020,** *11* (5), 732-739.

36. Lim, Y. C.; Desta, Z.; Flockhart, D. A.; Skaar, T. C., Endoxifen (4-hydroxy-N-desmethyl-tamoxifen) has anti-estrogenic effects in breast cancer cells with potency similar to 4-hydroxy-tamoxifen. *Cancer Chemother Pharmacol* **2005,** *55* (5), 471-8.
37. Abramoff, M. D.; Magelhaes, P. J.; Ram, S. J., Image Processing with ImageJ. *Biophotonics International* **2004,** *11* (7).
38. Janoš, P.; Spinello, A.; Magistrato, A., All-atom simulations to studying metallodrugs/target interactions. *Curr Opin Chem Biol* **2020,** *61*, 1-8.
39. Massova, I.; Kollman, P., Combined molecular mechanical and continuum solvent approach (MM-PBSA/GBSA) to predict ligand binding. *Perspectives in Drug Discovery and Design* **2000,** *18*, 113-135.
40. Miquel, J. F.; Olsson, K.; Sundbeck, B., Synthesis Of Unsymmetrical Diphenylalkenes. *J Med Chem* **1963,** *6*, 774-80.
41. Kawakami, J.; Kimura, K.; Yamaoka, M., A convenient synthesis of 4(5)-alkylacyl-1H-imidazoles from 4(5)-imidazolecarboxaldehyde. *Synthesis-Stuttgart* **2003,** (5), 677-680.
42. Iwasaki, S., Photochemistry of imidazolides. I. The photo-Fries-type rearrangement of N-substituted imidazoles. *Helv Chim Acta* **1976,** *59* (8), 2738-52.
43. Friesner, R. A.; Banks, J. L.; Murphy, R. B.; Halgren, T. A.; Klicic, J. J.; Mainz, D. T.; Repasky, M. P.; Knoll, E. H.; Shelley, M.; Perry, J. K.; Shaw, D. E.; Francis, P.; Shenkin, P. S., Glide: a new approach for rapid, accurate docking and scoring. 1. Method and assessment of docking accuracy. *J Med Chem* **2004,** *47* (7), 1739-49.
44. Maximov, P. Y.; Abderrahman, B.; Fanning, S. W.; Sengupta, S.; Fan, P.; Curpan, R. F.; Rincon, D. M. Q.; Greenland, J. A.; Rajan, S. S.; Greene, G. L.; Jordan, V. C., Endoxifen, 4-Hydroxytamoxifen and an Estrogenic Derivative Modulate Estrogen Receptor Complex Mediated Apoptosis in Breast Cancer. *Mol Pharmacol* **2018,** *94* (2), 812-822.
45. Spinello, A.; Pavlin, M.; Casalino, L.; Magistrato, A., A Dehydrogenase Dual Hydrogen Abstraction Mechanism Promotes Estrogen Biosynthesis: Can We Expand the Functional Annotation of the Aromatase Enzyme? *Chemistry* **2018,** *24* (42), 10840-10849.
46. Anandakrishnan, R.; Aguilar, B.; Onufriev, A. V., H++ 3.0: automating pK prediction and the preparation of biomolecular structures for atomistic molecular modeling and simulations. *Nucleic Acids Res* **2012,** *40* (Web Server issue), W537-41.
47. Di Nardo, G.; Breitner, M.; Bandino, A.; Ghosh, D.; Jennings, G. K.; Hackett, J. C.; Gilardi, G., Evidence for an elevated aspartate pK(a) in the active site of human aromatase. *J Biol Chem* **2015,** *290* (2), 1186-96.
48. Sgrignani, J.; Magistrato, A., Influence of the membrane lipophilic environment on the structure and on the substrate access/egress routes of the human aromatase enzyme. A computational study. *J Chem Inf Model* **2012,** *52* (6), 1595-606.
49. Wickstrom, L.; Okur, A.; Simmerling, C., Evaluating the performance of the ff99SB force field based on NMR scalar coupling data. *Biophys J* **2009,** *97* (3), 853-6.
50. Lindorff-Larsen, K.; Piana, S.; Palmo, K.; Maragakis, P.; Klepeis, J. L.; Dror, R. O.; Shaw, D. E., Improved side-chain torsion potentials for the Amber ff99SB protein force field. *Proteins* **2010,** *78* (8), 1950-8.
51. Shahrokh, K.; Orendt, A.; Yost, G. S.; Cheatham, T. E., Quantum mechanically derived AMBER-compatible heme parameters for various states of the cytochrome P450 catalytic cycle. *J Comput Chem* **2012,** *33* (2), 119-33.
52. Wang, J.; Wolf, R. M.; Caldwell, J. W.; Kollman, P. A.; Case, D. A., Development and testing of a general amber force field. *J Comput Chem* **2004,** *25* (9), 1157-74.

53. Bayly, C.; Cieplak, P.; Cornell, W.; Kollman, P., A Well-Behaved Electrostatic Potential Based Method Using Charge Restraints For Deriving Atomic Charges - The Resp Model. *Journal of Physical Chemistry* **1993,** *97* (40), 10269-10280.
54. Wang, J.; Wang, W.; Kollman, P. A.; Case, D. A., Automatic atom type and bond type perception in molecular mechanical calculations. *J Mol Graph Model* **2006,** *25* (2), 247-60.
55. Jorgensen, W. L.; Chandrasekhar; J.; Madura, J. D.; Impey, R. W.; Klein, M. L., Comparison of Simple Potential
Functions for Simulating Liquid Water. *J. Chem. Phys.* **1983,** *79*, 926-935.
56. Van Der Spoel, D.; Lindahl, E.; Hess, B.; Groenhof, G.; Mark, A. E.; Berendsen, H. J., GROMACS: fast, flexible, and free. *J Comput Chem* **2005,** *26* (16), 1701-18.
57. Bussi, G.; Donadio, D.; Parrinello, M., Canonical sampling through velocity rescaling. *Journal of Chemical Physics* **2007,** *126* (1).
58. Sgrignani, J.; Casalino, L.; Doro, F.; Spinello, A.; Magistrato, A., Can multiscale simulations unravel the function of metallo-enzymes to improve knowledge-based drug discovery? *Future Med Chem* **2019,** *11* (7), 771-791.
59. Spinello, A.; Magistrato, A., An omics perspective to the molecular mechanisms of anticancer metallo-drugs in the computational microscope era. *Expert Opin Drug Discov* **2017,** *12* (8), 813-825.
60. VandeVondele, J.; Krack, M.; Mohamed, F.; Parrinello, M.; Chassaing, T.; Hutter, J., QUICKSTEP: Fast and accurate density functional calculations using a mixed Gaussian and plane waves approach. *Computer Physics Communications* **2005,** *167* (2), 103-128.
61. Laino, T.; Mohamed, F.; Laio, A.; Parrinello, M., An efficient real space multigrid OM/MM electrostatic coupling. *Journal of Chemical Theory and Computation* **2005,** *1* (6), 1176-1184.
62. Laino, T.; Mohamed, F.; Laio, A.; Parrinello, M., An efficient linear-scaling electrostatic coupling for treating periodic boundary conditions in QM/MM simulations. *Journal of Chemical Theory and Computation* **2006,** *2* (5), 1370-1378.
63. Becke, A., Density-Functional Exchange-Energy Approximation With Correct Asymptotic-Behavior. *Physical Review a* **1988,** *38* (6), 3098-3100.
64. Lee, C.; Yang, W.; Parr, R., Development Of The Colle-Salvetti Correlation-Energy Formula Into A Functional Of The Electron-Density. *Physical Review B* **1988,** *37* (2), 785-789.
65. VandeVondele, J.; Hutter, J., Gaussian basis sets for accurate calculations on molecular systems in gas and condensed phases. *Journal of Chemical Physics* **2007,** *127* (11).
66. Goedecker, S.; Teter, M.; Hutter, J., Separable dual-space Gaussian pseudopotentials. *Physical Review B* **1996,** *54* (3), 1703-1710.
67. Hartwigsen, C.; Goedecker, S.; Hutter, J., Relativistic separable dual-space Gaussian pseudopotentials from H to Rn. *Physical Review B* **1998,** *58* (7), 3641-3662.
68. Sgrignani, J.; Iannuzzi, M.; Magistrato, A., Role of Water in the Puzzling Mechanism of the Final Aromatization Step Promoted by the Human Aromatase Enzyme. Insights from QM/MM MD Simulations. *Journal of Chemical Information and Modeling* **2015,** *55* (10), 2218-2226.
69. Ritacco, I.; Spinello, A.; Ippoliti, E.; Magistrato, A., Post-Translational Regulation of CYP450s Metabolism As Revealed by All-Atoms Simulations of the Aromatase Enzyme. *J Chem Inf Model* **2019,** *59* (6), 2930-2940.
70. Nose, S. A., Unified Formulation of the
Constant Temperature Molecular-Dynamics Methods. *J. Chem. Phys.* **1984,** *81*, 511-519.
71. Joung, I.; Cheatham, T., Determination of alkali and halide monovalent ion parameters for use in explicitly solvated biomolecular simulations. *Journal of Physical Chemistry B* **2008,** *112* (30), 9020-9041.
72. Daura, X.; Gademann, K.; Jaun, B.; Seebach, D.; van Gunsteren, W.; Mark, A., Peptide folding: When simulation meets experiment. *Angewandte Chemie-International Edition* **1999,** *38* (1-2), 236-240.

73. Casalino, L.; Palermo, G.; Spinello, A.; Rothlisberger, U.; Magistrato, A., All-atom simulations disentangle the functional dynamics underlying gene maturation in the intron lariat spliceosome. *Proceedings of the National Academy of Sciences of the United States of America* **2018,** *115* (26), 6584-6589.
74. Miller, B.; McGee, T.; Swails, J.; Homeyer, N.; Gohlke, H.; Roitberg, A., MMPBSA.py: An Efficient Program for End-State Free Energy Calculations. *Journal of Chemical Theory and Computation* **2012,** *8* (9), 3314-3321.
75. Nguyen, H.; Roe, D.; Simmerling, C., Improved Generalized Born Solvent Model Parameters for Protein Simulations. *Journal of Chemical Theory and Computation* **2013,** *9* (4), 2020-2034.
76. Genheden, S.; Ryde, U., The MM/PBSA and MM/GBSA methods to estimate ligand-binding affinities. *Expert Opinion on Drug Discovery* **2015,** *10* (5), 449-461.
77. Borisek, J.; Saltalamacchia, A.; Spinello, A.; Magistrato, A., Exploiting Cryo-EM Structural Information and All-Atom Simulations To Decrypt the Molecular Mechanism of Splicing Modulators. *Journal of Chemical Information and Modeling* **2020,** *60* (5), 2510-2521.
78. Humphrey, W.; Dalke, A.; Schulten, K., VMD: Visual molecular dynamics. *Journal of Molecular Graphics & Modelling* **1996,** *14* (1), 33-38.
79. Pettersen, E.; Goddard, T.; Huang, C.; Couch, G.; Greenblatt, D.; Meng, E.; Ferrin, T., UCSF chimera - A visualization system for exploratory research and analysis. *Journal of Computational Chemistry* **2004,** *25* (13), 1605-1612.